CONTINUOUS-FLOW PHOTOCATALYTIC TREATMENT OF PHARMACEUTICAL MICROPOLLUTANTS: ACTIVITY, INHIBITION, AND DEACTIVATION OF TiO_2 PHOTOCATALYSTS IN NATURAL WATER MATRICES

BY

SEAN CARBONARO

THESIS

Submitted in partial fulfillment of the requirements
for the degree of Master of Science in Environmental Engineering in Civil Engineering
in the Graduate College of the
University of Illinois at Urbana-Champaign, 2012

Urbana, Illinois

Adviser:

Professor Timothy J. Strathmann

ABSTRACT

Titanium dioxide (TiO_2) photocatalysts have been shown to be effective at degrading a wide range of organic micropollutants under ideal laboratory solution conditions (e.g., deionized water). However, little research has been performed regarding photocatalyst performance in more complex matrices representative of contaminated water sources (e.g., wastewater effluent, groundwater). Here, a benchtop continuous-flow reactor was developed for the purpose of studying the activity, inhibition, and deactivation of immobilized TiO_2 photocatalysts during water treatment applications. As a demonstration, degradation of four model pharmaceutical micropollutants (iopromide, acetaminophen, sulfamethoxazole, and carbamazepine) was monitored in both deionized water (DI), biologically treated wastewater effluent (WWE), and groundwater (GW) to study the effects of non-target constituents present in the latter matrix. Reactor performance was shown to be sufficiently stable over 7 days when treating micropollutants in DI. When reactor influent was switched WWE, photocatalytic degradation of individual micropollutants was inhibited to varying degrees, ranging from 42 to 86%. However, most of the catalyst activity was recovered upon switching back to the DI matrix after 4 d, suggesting mostly competitive inhibition of the photocatalysts by WWE matrix components (e.g., effluent organic matter scavenging of ·OH) rather than irreversible catalyst deactivation. Experiments conducted using pretreated WWE and synthetic WWE mimic solutions indicated that both organic and inorganic constituents in WWE contributed to the observed catalyst inhibition. Analysis of immobilized TiO_2 thin films after 4 d of continuous treatment of the WWE matrix indicated minor deterioration of the porous thin film. Photocatalytic degradation rates of micropollutants displayed different trends on a GW-exposed photocatalyst. Easily oxidizable compounds (acetaminophen and sulfamethoxazole) were little affected by catalyst

exposure to GW, while more recalcitrant compounds (iopromide and carbamazepine) were significantly inhibited. Significant calcium precipitation was found on the catalyst using SEM-EDS. Oxalic acid was found to be an effective rinsing solution of the catalyst. It is suspected that calcium, manganese, and iron are the primary groundwater constituents responsible for catalyst deactivation, but further tests are needed to confirm. Results demonstrate the marked influence of non-target constituents present in complex matrices on long-term catalyst activity and highlight the need for increased study of this important issue to further the development of practical photocatalytic water treatment technologies.

ACKNOWLEDGEMENTS

This work was supported by a National Science Foundation CAREER Award to T. Strathmann (CBET 07-46453) and the Global Collaborative Research Office of King Abdullah University of Science and Technology (KAUST) through the Collaborative Research on Sustainable Water Development and Engineering Partnership. Materials characterization was carried out in part in the Frederick Seitz Materials Research Laboratory Central Facilities, University of Illinois. I would like to thank Matthew Sugihara and Laura Asmuth for building dipcoating and reactor devices and assistance in developing laboratory procedures. I would like to thank Shaoying Qi for his technical help on a number of techniques and processes used throughout this research.

TABLE OF CONTENTS

INTRODUCTION

Though pharmaceutical use has improved the quality of human life, a large fraction of administered drugs are excreted by consumers and many of these chemicals have been found to be recalcitrant to conventional wastewater treatment processes).[1] As a result, many pharmaceuticals and personal care products have been detected as micropollutants in water supplies that receive inputs from wastewater treatment plants.[2] Although concentrations of these micropollutants are very low, usually ng/L to µg/L, concerns have been raised because little is known about the effects of chronic exposure to mixtures of these chemicals by sensitive aquatic organisms present.[3,4] Human health concerns have also been raised, particularly in areas that have instituted recycled potable water programs (e.g., California, Arizona, and Florida), where potential exists for accumulation of persistent micropollutants as well as biologically active metabolites and degradates.[4]

Concerns about the occurrence chemically diverse micropollutants have increased interest in the development of advanced treatment technologies capable of eliminating a wide spectrum of micropollutants prior to discharge or reuse of biologically treated wastewater effluent. A number of advanced oxidation processes (AOPs) are promising treatment options.[5,6] Collectively, AOPs generate hydroxyl radical (·OH) which reacts non-selectively with most organic pollutants at near diffusion-limited conditions (e.g., k_2 values from 10^8 – 10^{10} M^{-1} s^{-1} at 25°C [7]). For some highly recalcitrant micropollutants like iodinated X-ray contrast media, AOPs are the only treatment option available other than most energy-intensive membrane processes. [8–10]

Titanium dioxide (TiO_2) photocatalysis is a promising AOP that has demonstrated ability to transform or degrade many micropollutants (**Figure 1**).[11–13] Irradiation of TiO_2 with ultraviolet (UV) light exceeding the semiconductor bandgap energy (E_g = 3.10 eV and 3.23 eV for rutile and anatase, respectively, corresponding to λ < 400 and 384 nm, again respectively [14]) excites electrons from a filled valence band to an empty conduction band, creating electron-hole pairs. The valence band holes (h_{vb}^+) can initiate oxidative pathways (e.g., reacting with adsorbed H_2O to produce ·OH), while conduction band electrons (e_{cb}^-) can react with adsorbed O_2 or other electron-accepting species, including some contaminants.[15] Advantages of photocatalytic treatment processes include the low cost, chemical stability, and biological and chemical inertness TiO_2 materials [16], and the potential use of solar irradiation.[17] Many current research

efforts are aimed at modifying TiO_2 materials to expand their active range into visible regions of the solar spectrum ($\lambda > 400$ nm).[18]

Although a large body of literature has demonstrated that UV-TiO_2 photocatalysis processes are effective for transforming organic pollutants, the vast majority of studies have been conducted under idealized conditions using experimental systems that do not permit easy translation of results to more practical engineered treatment operations. Most experimental studies have been conducted in batch systems where suspensions of TiO_2 nanoparticles are irradiated [12,19–21], whereas catalysts will likely need to be immobilized on fixed support materials and contaminated water will be treated in a continuous-flow configuration in engineered treatment processes. Most experimental studies have also focused on elucidation of detailed reaction kinetics and pathways for individual contaminants, and thus experiments were conducted using micropollutant concentrations (e.g., >1 mg/L) that are far greater than those measured in real water matrices (e.g., ng/L – μg/L), and target micropollutants are studied in the absence of non-target water constituents that are typically present in natural water matrices at orders-of-magnitude higher concentration (e.g., natural organic matter, dissolved carbonate species and other major ions).[11,22] Some studies have attempted to address these issues by studying photocatalytic treatment of micropollutants in natural water matrices or laboratory waters amended with important non-target constituents; however, the practical application of findings from these efforts is often limited because studies were conducted under artificial conditions where the target micropollutant concentration actually exceeds the non-target constituent concentration, which poorly represents treatment scenarios where non-target constituents are likely to represent the majority of dissolved solids and organic matter and will act to scavenge a major fraction of reactive species generated by photocatalysts. Finally, batch experimental systems are inappropriate for studying the long-term activity of catalysts during real treatment operations where catalysts will be continuously exposed to a new feed stream of water that may contain low levels of catalyst-reacting constituents that may progressively deactivate catalysts over time. Instead, continuous-flow experimental setups at varying scales are needed to examine these factors.

To begin addressing some of these critical issues, here we describe the development of a laboratory benchtop continuous-flow photocatalyst reactor system that can be used to study catalyst activity, stability, inhibition and deactivation during continuous treatment of target

micropollutants in both laboratory solution and natural water matrices relevant to the water treatment industry. Commercial TiO_2 nanoparticles were immobilized as thin films on glass supports (microscope slides) placed in a serpentine plug flow reactor and irradiated by commercial UV-A light sources (**Figure 2**). While the reactor is not intended to replicate all the complexity of actual field-scale engineered processes, the laboratory-scale reactor enables preliminary investigation of factors that will be critical to the success of larger scale treatment processes (e.g., catalyst stability, inhibition, deactivation, and potential regeneration of fouled catalysts). Immobilization of catalysts on microscope slides also facilitates analysis of the effects of treatment operations and matrix exposure on catalyst properties. In this contribution, we first established the stability and reproducibility of reactor performance through long-term (e.g., 1 week) continuous-flow experiments where a mixture of four pharmaceutical micropollutants are treated in pH-buffered deionized (DI) water solution. The performance of the reactor using a tertiary treated wastewater effluent (WWE) and a groundwater (GW) matrix were also examined as model natural water matrices because of the interest in applying photocatalysis as an advanced treatment option for micropollutants that are recalcitrant to biological wastewater treatment processes. Photocatalytic treatment of a mixture of four widely detected pharmaceutical micropollutants was examined (**Figure 3**). Individual compounds were selected as model micropollutants because of their expected recalcitrance to other wastewater treatment processes [1] and their documented transformation by TiO_2 photocatalysis.[12,19,23]

EXPERIMENTAL METHODS

2.1. Supplies

All chemicals were reagent grade and were used as received from Sigma-Aldrich-Fluka or Fisher, unless otherwise indicated. Iopromide was provided as a gift from Schering AG (Berlin, Germany). Nanophase TiO_2 (primary particle size of 30 nm) composed of a mixture of anatase and rutile phases (Type P25, 50 m^2 g^{-1}) was provided by Degussa.[24] Granular activated carbon (GAC; Filtrasorb 820) was obtained from Calgon Carbon Corporation. WWE was obtained from the outfall of the Urbana-Champaign Sanitary District (UCSD) Northeast Wastewater Treatment Facility. Prior to use, WWE was filtered sequentially with 10 μm and 1 μm membrane filters (Polygard-CR 10 μm and Lifegard 1 μm, Millipore) and stored under darkness at 4°C. Groundwater (GW) was obtained from a well beneath Newmark Civil Engineering Building. Prior to use, GW was aerated for 2 hours then filtered like the WWE. Deionized water (Barnstead NANOpure systems; >18 MΩ·cm resistivity) was used to prepare all other solutions.

2.2. Immobilized TiO_2 thin films

Immobilized porous thin films of TiO_2 were produced using a procedure modified from that described by Balasubramanian and coworkers (2003).[25] Thirty g/L of TiO_2 nanoparticles (Degussa P25) were mixed into a TiO_2 sol-gel containing 0.42 M titanium isopropoxide (TTIP), 1.68 M diethanolamine, and 0.84 M water in isopropanol. Glass microscope slides (**Figure 4A**; 75 mm × 25 mm × 1 mm; Thermo Scientific Gold Seal) were used as a substrate for depositing the thin films in place of the stainless steel used by Balasubramanian and coworkers. An automated dipcoating apparatus was designed to hold five glass slides vertically and lift out of the sol gel mixture at a uniform rate of 20 cm/min. The coated slides were then placed on a rack and dried at room temperature for 24 h before heat treating in a programmable furnace. Heat treatment consisted of heating slides at 3°C/min to 100°C, holding for 1 h, then increasing at 3°C/min to 600°C, again holding for 1 h before cooling to ambient temperature. Three dip coating/heat treatment cycles were used on each substrate, as initial tests indicated no further improvement in photocatalytic activity with application of additional coatings.

2.3. Continuous-flow reactor

The activity of immobilized photocatalyst thin films was studied in a serpentine-pattern plug flow reactor, pictured in **Figure 2**. The reactor was designed to have five channels, each the width of 1 standard microscope slide (25 mm) and length of 5 slides (75 mm each), for a total of 25 film-coated slides along the entire reactor flow path. Five 15 W 18" long UV-A lamps with spectrum centered at ~365 nm (manufactured by General Electric) were suspended and centered over each of the five channels (12 cm between lamp and film-coated slides). Inlet flow rate was controlled using a Masterflex L/S digital standard drive peristaltic pump**,** and reactor volume can be controlled by placing weirs of varying height at the end of the plug flow reactor. Unless otherwise noted, a mean flow rate of 2.7 mL/min and weir height of 0.62 cm were used, resulting in a reactor volume of 325 mL and a theoretical hydraulic residence time of 120 min. The design residence time was selected to achieve between 50-90% degradation of the target micropollutants in a clean DI water matrix based upon preliminary test measurements of the immobilized catalyst activity under circulating batch conditions. Designing based upon this range of micropollutant degradation permitted better quantification of matrix effects than if design was based upon a higher level of treatment where changes in catalyst activity would be more difficult to quantify.

2.4. Reactor and catalyst characterization

Tracer studies were conducted using perchlorate, a photocatalytically inert species, to determine flow patterns. A pulse addition of $NaClO_4$ (5 mL of 5 mg/L) was introduced to the reactor influent (DI water), and then samples were periodically collected for analysis at a point directly before the outlet weir to monitor tracer breakthrough. Collected samples were filtered (0.22 μm cellulose acetate) and analyzed by ion chromatography (IC).

Potassium ferrioxalate actinometry [26] was used to quantify UVA flux incident on the reactor. UVA lamps were allowed to warm up for >1 h prior to measurement. Three solutions were prepared separately immediately before measurement: 87.5 mL of 0.3 M $Fe_2(SO_4)_3$, 87.5 mL of 1.8 M K-oxalate, and 175 mL of 0.2 N H_2SO_4. The solutions were then mixed together outside of the lamps for 10 s, then quickly added to the reactor (containing glass slides with no TiO_2 coating) under the lamps. The contents of the reactor were then rapidly circulated by pump (166 mL/min) by connecting the reactor outlet and inlet with tubing. Ten samples (60 μL) were then

collected at regular intervals for 15 min, mixed with 4.94 mL of a ferrozine colorimetric agent solution (0.4 g/L buffered at pH 7 with 0.06 M MOPS), and analyzed by spectrophotometer at λ = 562 nm. Four replicate experiments yielded a photon flux was $9.31(\pm 1.62)\times 10^{-7}$ E/s (see Appendix A).

Several procedures were used to characterize the photocatalyst films before and after exposure to different water matrices. Film thickness was measured using profilometry (Sloan Dektak[3]) after etching a cross section out of thin film with a razor blade [3]. Average thickness was determined by analysis of 3 parallel (across same etch) surface scans of 3.5 mm length collected for 3 replicate films for each type (e.g., virgin, WWE-exposed). A stylus tracking force of 15 mg was applied for profilometry analysis. X-ray diffraction (XRD) analysis of the immobilized films was conducted using a Panalytic/Philips X'Pert MRD system using Cu Kα radiation, and crystalline phases were determined by comparison against the Powder Diffraction File (PDF) database. X-ray photoelectron spectroscopy (XPS) measurements were collected using a Physical Electrons PHI 5400. Energy-normalization of the spectra was accomplished by shifting the C 1s peak to 285 eV. Survey data presented in the paper were captured by 5 passes collected over 12 minutes. Scanning electron microscopy with energy dispersive X-ray spectroscopy (SEM-EDS) was performed using a JEOL JSM-6060LV. Samples were sputter-coated with Au/Pd or C prior to analysis.

2.5. Batch micropollutant treatment experiments

Micropollutant treatment experiments, both with and without TiO_2 catalysts present, were conducted in the reactor operated in circulating batch mode. In these experiments, after allowing lamps to warm up for >1 h, the reactor contents were first filled with 325 mL of water initially containing 50 µg/L of each target micropollutant. The micropollutant-spiked DI water was buffered at pH 8.2 and 10 mM ionic strength (1 mM $NaHCO_3$ + 9 mM NaCl); these conditions will hereafter be referred to as the "DI water" matrix. The pH value was selected to match the WWE matrix used in later experiments. Reactor influent and effluent channels were closed and the reactor contents were circulated from the effluent to influent ends at a rate of 166 mL/min. Aliquots (1 mL) of the reactor solution were then periodically collected for analysis of micropollutant concentrations from the center of the middle lane. Results were used to quantify the relative photocatalytic reactivity of individual micropollutants in the absence of interfering

matrix constituents. Results from catalyst-free batch reactions were also used to assess the potential importance of UV-A direct photolysis processes for degradation of target micropollutants.

Experiments were conducted using initial micropollutant concentrations of 50 μg/L of each compound. This value was selected because it was low enough to represent only a small (<5%) fraction of the total dissolved organic carbon (DOC) present when treating natural water matrices like the WWE used here, but high enough to permit quantification of treated solutions (where C_{eff} is only a few μg/L in some cases) by liquid chromatography-tandem mass spectrometry (LC-MS/MS) analysis without matrix interferences or need for pre-concentration by solid phase extraction. Thus, although the spiked concentrations significantly exceed those typically detected in wastewater effluent (often <0.1 μg/L) [2], they are still low enough to be considered only minor solution constituents, and so similar matrix effects can be expected.

2.6. Continuous-flow micropollutant treatment experiments

Continuous-flow micropollutant treatment experiments were conducted to evaluate long-term activity of photocatalysts as well as the effects of treating micropollutants present in WWE containing high levels of effluent organic matter (EfOM) and other inorganic constituents. Experiments were initiated in a similar manner as the batch experiments. After allowing lamps to warm up, treatment experiments were begun by irradiating the reactor initially filled with 325 mL of the desired feed solution spiked with the four target pharmaceutical micropollutants (50 μg/L each). Fresh micropollutant feed solution was then added to the influent end of the reactor at the desired flow rate (typically 2.7 mL/min) and effluent was released by flow over the outlet weir. Samples of influent and effluent were then periodically collected for analysis to determine the fraction of each target micropollutant remaining following photocatalytic treatment (C_{eff}/C_{inf}). Flow rates were checked by volumetric analysis of reactor effluent measured for a length of time (>2 h). Effluent samples were collected by syringe filter from a location immediately in front of the effluent weir. Between six and eight effluent samples per operating day were collected. Influent samples were collected by syringe filter from the influent feed reservoir in use on that particular operating day. Only one influent sample per operating day was collected because measurements showed this value to be stable.

Initially, photocatalytic treatment of micropollutants was evaluated in DI water matrix. Short-term experiments were conducted to assess the time needed to reach steady-state effluent concentrations and compare the relative reactivity of individual micropollutants with that observed when the reactor was operated in circulating batch mode. Continuous treatment of micropollutants in the DI water matrix was then monitored for 7 d to evaluate overall reactor and catalyst stability.

Experiments evaluating the effects of natural water matrices (NWM) on photocatalytic treatment of the target micropollutants were conducted in three stages. Experiments were initiated with the DI water matrix as described above, and micropollutant treatment in the DI water matrix was monitored for 24 h to 48 h to establish a baseline steady-state treatment level. Then, the influent feed solution was switched to micropollutant-spiked NWM, and treatment of the micropollutants was monitored 96 h. Finally, the influent feed solution was switched back to the micropollutant-spiked DI water matrix and monitored for another 48 h to evaluate to what extent catalyst activity returned to pre-NWM treatment levels.

Similar experiments were also conducted using WWE pre-treated with GAC to assess the effects of reducing DOC levels in the WWE matrix. WWE was pretreated by equilibrating 17 L of the matrix with 68 g of GAC in a stirred batch reactor for 24 h before re-filtering (Whatman 2.5 μm circle filter paper) and spiking with target micropollutants. A synthetic mimic WWE with only the major inorganic components (≥10 μg/L) in the WWE ("Inorganic WWE mimic") was also prepared and used as reactor influent to assess the effects of constituents other than EfOM on catalyst activity. As mentioned previously, groundwater was aerated for 2 h prior to filtration. This was considered a necessary pretreatment as the non-aerated groundwater contained 0.45 mg/L iron, and aeration followed by filtration reduced this to 0.061 mg/L. Alkalinity was also reduced from 240 mg/L $CaCO_3$ to 200 mg/L $CaCO_3$. Preliminary experiments indicated reduction of these values were helpful in delaying and/or reducing precipitation on the catalyst surface. For one experiment, groundwater was softened following aeration by adding NaOH to raise to pH 11, the filtering (1 μm) to remove CaCO3, then re-adjusting the pH to the original value (pH 8.3) with HCl.

2.7. Analytical

Quantitative analysis of the four micropollutants was LC-MS/MS (Agilent 1200 Series LC, Agilent LC/MSD Trap XCT Ultra). A Zorbax Eclipse XDB-C18 column (2.1×50 mm, 3.5 μm particle size) was used as the stationary phase and a gradient mobile phase (0.2 mL/min) was used with two solvents (A: 95% water, 5% acetonitrile, and 0.1% formic acid; B: 5% water, 95% acetonitrile, and 0.1% formic acid). Following injection, solvent B was increased from 0 to 60% over 10 min, then from 60 to 100% over the next 10 min, then decreased back to 0% over the next 0.1 min and held constant for 12 min. Individual micropollutants were quantified by selective ion monitoring mode with the following retention times and ion transitions: IOP (16.7 min, m/z 792 → 573); APAP (17.5 min, m/z 152 → 110); SMX (22.5 min, m/z 254 → 156); CBZ (23.5 min, m/z 237 → 194). Limits of quantification (LOQ) in the WWE were approximately 0.5 μg/L for each micropollutant. Perchlorate was quantified by ion chromatography analysis with conductivity detection (IC-CD; Dionex ICS-2000, 100 μL sample loop, Dionex IonPac AS16 column, 36 mM KOH eluent, 1 mL/min eluent flow rate).

Major water quality parameters for the WWE and GW (pH, alkalinity, TDS) were determined according to *Standard Methods for the Examination of Water and Wastewater* [27]. Major anions were analyzed by IC-CD (Dionex IonPac AS18 column). Metals analysis was conducted by inductively coupled plasma-mass spectrometry (ICP-MS; Perkin Elmer Sciex Elen DRCe). Additional Mn and Fe tests were performed using Hach kits. Dissolved organic carbon (DOC) was measured using a Shimadzu TOC-VCPH combustion analyzer.

RESULTS AND DISCUSSION

3.1. Catalyst characterization

Figure 4 summarizes the characterization of the immobilized TiO_2 thin films. SEM analysis of the films (**Figure 4C-D**) yielded similar features to those reported by Balasubramanian and coworkers.[28] The grain size in the porous film was roughly 100-200 nm. We also noted the development of microcracks in the film surface. Agglomerates of TiO_2 on the order of 1-10 μm also formed on the surface of films.[29] EDS analysis (not shown) showed primarily Ti, O and C on the surface.

Profilometry analysis (**Figure 4B**) indicated an average thickness for the porous TiO_2 films of 1.30(±0.34) μm after 3 dipcoating/heat treatment cycles. This compares with an average primary particle size for Degussa P25 of 30 nm.[24] When using a similar dipcoating procedure, Balasubramanian et al (2004) achieved a thickness of 110 μm from 3 coating/heat treatment cycles on a stainless steel support [28], approximately 85 times the thickness observed here.

Quantitative analysis of the X-ray diffraction data (**Figure 4E**) indicated that the film contained a crystalline component composed of 78% anatase and 22% rutile. This is consistent with previous reports of Degussa P25.[28] The crystallite size of anatase and rutile were 196 Å and 347 Å, respectively. These results compare reasonably well with that reported by Balasubramanian and coworkers [28], with major differences being attributed to the support substrate (glass versus stainless steel).

Prominent peaks observed with XPS analysis (**Figure 4F**) included Ti 2p, O 1s, and C 1s, consistent with the elements observed with SEM-EDS. The double peak of Ti 2p was expected for TiO_2. The C 1s comes from the incomplete pyrolysis of diethanolamine and isopropanol during heat treatment of immobilized sol.[29] Chen and Dionysiou [29] observed the same XPS peaks. In addition, these authors observed foreign metals including Cr, Fe and Mn on the surface, which was attributed to the stainless steel support used.

3.2. Reactor characteristics

Conservative tracer and batch treatment experiments were first conducted to separately characterize the hydraulic and photocatalytic properties in the reactor system. **Figure 5A** shows the result of a tracer experiment. Effluent concentrations of perchlorate began to be detected ~70 min after pulse input of $NaClO_4$, then increased to a peak value at ~100 min before slowly decreasing to non-detectable levels by ~190 min. Calculation of the mean residence time yielded a value of 117 min [30], which agrees with the theoretical residence time of 120 min (V/Q = 325 mL / 2.7 mL/min = 120 min). The Péclet and Reynolds numbers were found to be 44.2 and 9.3, respectively, and the longitudinal dispersion coefficient of the tracer was determined to be 1.65×10^{-2} cm^2 min^{-1}.

Figure 6 shows timecourses for photocatalytic degradation of the four target micropollutants in replicate experiments measured in buffered DI water where the reactor was operated in high flowrate (166 mL/min) circulating batch mode. Degradation of all four compounds could be described by a first-order rate law and model fits yielded observed rate constants that vary from IOP (k_{obs} = 0.41 h^{-1}) < SMX ~ CBZ (0.5 h^{-1}) < APAP (0.83 h^{-1}). We expect these measured k_{obs} values to be the maximum degradation rate constants at the selected solution conditions and water depth overlying the catalyst films. The only expected competing species for photocatalytically generated ·OH was the bicarbonate ions added to buffer pH. A catalyst-free photolysis control experiment was also conducted to assess the potential relevance of direct photolysis reactions. Minimal degradation of the target micropollutants was observed in the circulating reactor within 6 h (k_{obs} < 0.02 h^{-1}), indicating negligible contribution to the micropollutant losses observed during photocatalytic treatment.

No comparable studies using thin-film TiO_2 photocatalysts for degrading these micropollutants are available for comparing reactivity trends. However, relative reactivity trends of the same micropollutants have been noted in studies conducted in TiO_2 suspensions. Miranda-García and coworkers [23] observed similar photocatalytic degradation rates for SMX and CBZ (differ by <10%) in UV-irradiated suspensions of TiO_2, in agreement with the trend observed here. Like here, Doll and Frimmel [12] also observed similar reactivities for CBZ and iomeprol (structurally related to iopromide) in batch suspensions of P25 TiO_2 (rates differ by ~16%). Finally, Klamerth and coworkers [19] reported slower photocatalytic degradation of SMX compared to APAP.

3.3. Continuous-flow treatment: steady-state operation and reactor stability

Continuous-flow experiments (i.e., single pass of reactor influent) were first conducted in the same DI water matrix used for batch experiments. Initially, the reactor was filled with solution containing 50 μg/L of each micropollutant, and tests showed that after initiating irradiation and flow conditions, reactor effluent concentrations of each micropollutant decreased over the first 4 h until a steady level was approached, as shown for IOP in **Figure 5B**. Subsequently, monitoring of reaction effluent was begun after allowing ~12 h of continuous treatment to ensure that steady-state conditions had been reached.

Previous tests in batch systems demonstrated minimal degradation of micropollutants in catalyst-free solutions irradiated for 6 h, and continuous-flow dark control experiments indicated no detectable loss of micropollutants in the absence of UV-A irradiation (e.g., by adsorption to the catalyst films) over a 6 h period. Thus, it can be concluded that UV-TiO_2 photocatalytic processes are responsible for the observed micropollutant losses in the reactor effluent.

To evaluate long-term catalyst and reactor stability in the absence of complicating solution conditions, micropollutant treatment in the DI water matrix was monitored for 7 d. **Figure 7** shows the treatment level achieved for each micropollutant over the course of the experiment, with mean and standard deviation values indicated. Overall, the level of treatment for all four target micropollutants was stable over the entire period monitored, with no clear trends indicating decreases or increases in reactor performance due to extended use of photocatalysts or lamps. Tests also show that flow rates remain stable over the monitored period. Mean levels of treatment range from to 62% removal of IOP and CBZ to 84% removal of APAP, with variations around the mean values falling between 6-8%. Profilometry analysis of catalyst films showed no effect of catalyst use for 7 d on the film thickness or roughness, indicating physical stability of the films under hydraulic and irradiation conditions used in this study.

Figure 8 shows the k_{obs} values derived from the continuous-flow treatment experiments (**Figure 7**) with values obtained from first-order model fits to the batch treatment data (**Figure 6**). The former were calculated from the measured steady-state effluent and influent concentrations by assuming ideal plug flow with a mean residence time (τ) of 117 min, determined from tracer studies (**Figure 5A**):

$$k_{\text{obs}} = \frac{-\ln(\frac{C_{\text{eff}}}{C_{\text{inf}}})}{\tau} \quad (1)$$

In general, the values compared favorably for all four compounds, with some difference being noted for SMX. The general agreement confirms the mean residence time and reactor kinetics. The close match also confirms the validity of using continuous-flow treatment data to assess the activity of photocatalysts with different micropollutants. It follows that it may also be useful for quantifying catalyst inhibition and deactivation by non-target matrix constituents. In addition, it is worth noting that the close agreement between k_{obs} values determined under high and low flow-rate operation modes (166 mL/min for circulating batch versus 2.7 mL/min for continuous-flow modes) demonstrates that rates of micropollutant oxidation are independent of flow rates and not limited by mass transfer through a fluid boundary layer next to the photocatalyst films.

3.4. Photocatalytic treatment of micropollutant in WWE

Major characteristics of the WWE are shown in **Table 1**. Of particular importance, the WWE contained a significant DOC level (5.7 mg C/L), so addition of the four micropollutants increased DOC by <2% (107 µg/L) and did not affect bulk properties of the matrix. The WWE also contained a number of inorganic constituents, and the measured pH and alkalinity levels were suggestive of a similar level of dissolved bicarbonate as the buffered DI water solutions.

Figure 9 shows the results of representative continuous-flow treatment experiments for each of the target micropollutants. The vertical dashed lines separate each of the three treatment regimes. After establishing steady-state levels of micropollutant treatment in the DI water matrix over the first 24 h, the influent was switched to the WWE matrix for the next 96 h, followed by a return to the DI water for the final 48 h. For all four target micropollutants, the efficiency of treatment through the reactor decreased upon switching the reactor feed to the WWE matrix, but the extent of the decrease varied among the micropollutants. The largest effect occurred for IOP, where the level of treatment decreased from 64% removal from DI water to just 18% removal from WWE. In contrast, comparable matrix changes only decreased the mean level of SMX removal from 72% to 51%. It is also worth noting that little removal of the overall DOC (<5%) was observed during photocatalytic treatment, consistent with expectations that mineralization of organics only occurs upon extended exposure to AOPs.

Somewhat surprisingly, treatment efficiencies largely returned to the pre-WWE levels when the feed solution was switched back to DI water after 4 days of treating the micropollutants in WWE. **Figure 10** compares the mean rate constants observed for each of the three treatment regimes (eq 1). The rate constants are reduced in the WWE matrix to varying degrees as expected from the raw data in Figure 9, but the decrease is largely erased upon switching back to DI water, suggesting that most of the observed decreases in micropollutant treatment are reversible over the timescale of the experiments conducted here. This suggests that constituents in the WWE were inhibiting photocatalyst reactions with the target micropollutants, but were not acting to irreversibly deactivate the photocatalyst materials over the time period examined. Further studies are needed to assess the effects of longer-term photocatalyst exposure to the WWE matrix. The extent of inhibition can be calculated as the difference in reaction rate constants between the initial buffered DI solution and WWE matrix. The more easily oxidized compounds (APAP and SMX) were less inhibited in the WWE matrix than the more recalcitrant compounds (IOP and CBZ). This may result, in part, from the presence of electron-rich phenolic and aniline groups in the APAP and SMX structures, respectively, that are oxidizable by a wider range of oxidant species that might be formed in reactor (e.g., $CO_3{\cdot}^-$, $O_2{\cdot}^-$ [31]).

3.5. Identifying catalyst-inhibiting constituents in WWE

Although the WWE matrix contains a large number of constituents that might influence photocatalytic reactions with the target micropollutants, previous studies suggest that the effluent organic matter may be playing a prominent role in the observed inhibition. Dissolved organic matter can affect photocatalytic treatment processes in several ways [12]: (1) act a competitive scavenger of ·OH to reduce the effective concentration available for reacting with the target micropollutants, (2) competitively inhibit adsorption of the target micropollutants, thereby reducing interactions with adsorbed ·OH, and (3) absorb incident photons, reducing the available UV-A photon flux for TiO_2 excitation (i.e., screening). That said, results of continuous-flow treatment experiments showed only a small effect of GAC removal of DOC from the WWE. DOC in the WWE was reduced from 5.7 mg C/L to 1.4 mg C/L when pretreated with 4 g/L GAC. Despite the 75% reduction in DOC, the mean k_{obs} values for 2 of the 4 micropollutants measured in WWE were little affected (**Figure 11A**). This finding suggests that either EfOM is not the only constituent responsible for inhibition of photocatalysts in WWE or that the EfOM

fraction not removed by GAC adsorption was more catalyst inhibiting than the fraction that was removed. It would not be surprising that the EfOM constituents that are most surface reactive with a polar metal oxide like TiO_2 would be less amenable to adsorption by non-polar GAC. However, further research is needed before making such conclusions.

The role of non-DOM constituents in WWE was evaluated separately by examining micropollutant treatment in a laboratory "mimic" solution of the major inorganic components of the WWE described in **Table 1**. Results of these experiments show that micropollutant treatment is inhibited somewhat relative to buffered DI water, but to a lesser extent than in the WWE that also contains EfOM. Several of the inorganic species in the WWE have been shown to inhibit photocatalytic processes, including dissolved carbonate and phosphate species, Cl^-, NO_3^-, SO_4^{2-}, and metal ions like Fe and Mn.[34,35] Thus, these results suggest that both organic and inorganic constituents in the WWE are contributing to the observed inhibition of micropollutant removal, and further studies will be needed to identify those individual constituents that inhibit photocatalysts and evaluate the merits of pretreating WWE to selectively remove these constituents prior to catalyst treatment.

3.6. Catalyst deactivation and properties post-treatment in WWE

Although most of observed inhibition of photocatalysts appears reversible, at least on the timescale of experiments conducted here, close examination of the raw data (**Figure 9**) shows that a small fraction of the decrease in photocatalyst activity observed when treating micropollutants in the WWE matrix is not recovered when the influent is switched back to DI water matrix. With the exception of CBZ, the unrecovered losses in activity fall within the uncertainty of replicate measurements. For CBZ, the unrecovered loss in k_{obs} represents a 27% loss in catalyst activity. This result suggests that continuous catalyst exposure to WWE during treatment might also contribute to deactivation of the catalyst. Future studies will examine if the level of unrecovered losses in activity increase with increasing exposure time to the WWE matrix, and test catalyst washing strategies for regaining the losses in activity.

TiO_2 films were also re-characterized following exposure to the WWE matrix under treatment conditions for several days. No large changes in the bulk crystal structure or surface chemistry of the films were noted from XRD and XPS analysis, respectively. Visually, a slight brown discoloration developed on the WWE-exposed films. Profilometry analysis exhibited a

slight increase in film thickness (1.84±0.61 μm), but the difference was not statistically significant. SEM analysis showed that microcracks that were clearly visible in the virgin films (**Figure 4C-D**) were partially filled in following exposure to WWE, and other debris began to appear on the surface of films (**Figure 12B**). EDS analysis indicated most of the surface debris was TiO_2, suggesting some minor matrix-promoted deterioration of the film occurred. Markedly less deterioration was evident in TiO_2 thin films following treatment of the DI water matrix for 7 d. EDS and XPS analysis also indicated the presence of carbon in all three sample types, but this may be due to the presence of residual solvent from the sol-gel process. There was also a sparse amount of small (1 to 10 μm) Al and Ca-rich precipitates on the surface, possibly calcium carbonate. A sample precipitate with EDX spectra of the precipitate and background film is shown in **Figure 13**.

3.7. Photocatalytic treatment of micropollutant in GW

The major properties of aerated GW were characterized as described in the Experimental Methods. The major properties are listed in Table 2. The DI water matrix for use in GW exposure experiments was adjusted accordingly (3 mM $NaHCO_3$ + 9 mM NaCl).

Figure 14 shows the results of representative continuous-flow treatment experiments for each of the target micropollutants in aerated GW. The vertical dashed lines separate each of the three treatment regimes. After establishing steady-state levels of micropollutant treatment in the DI water matrix over the first 48 h, the influent was switched to the GW matrix for the next 96 h, followed by a return to the DI water for the final 48 h. The behavior of the photocatalysts in response to GW exposure was quite different from that in response to WWE exposure. The more recalcitratnt compounds (CBZ and IOP) were progressively inhibited over roughly the first 24 h before reaching a new steady state. Upon returning to the DI matrix, removal of these two compounds did not significantly improve, indicating the GW matrix does not necessarily just act competitively to inhibit the reactions (e.g., by radical scavenging), but instead acts to more irreversibly deactivate the catalyst towards reaction with these compounds. However, the rates of APAP and SMX were unaffected by the GW matrix. This suggests that different compounds will react predominantly by different mechanisms or at different types of reaction sites. APAP and SMX contain electron-rich phenolic and aniline functional groups that are oxidized by a wide range of oxidizing species, so may be less sensitive to deactivation than IOP and CBZ. It has

been reported that oxo-quinolinecarboxylic acid groups can react by a visible-light mediated mechanism with TiO_2.[32] APAP contains a similar group in its structure and may react by a related mechanism. This mechanism may not be affected by surface precipitation as other mechanisms like hydroxyl radical generation may be. SMX even exhibited decreased degradation rates upon return to the DI water matrix, indicating possible sensitization by the GW.

3.8. Catalyst deactivation and properties post-treatment in GW

Exposure to GW changed the properties of the photocatalysts. The change in activity was noted above. A brown film developed on the catalysts over the exposure time to the GW. This was suspected to be Mn and/or Fe, due to their relatively high concentrations (0.03 mg/L and 0.06 mg/L, respectively), and previous observations by Burns et al (1999).[33] However, to date, their presence has not been confirmed by XRD, XPS, or SEM-EDS. Burns et al (1999) reported that the Fe and Mn descended through the film to the titania/silica interface, possibly explaining why the more surface-sensitive methods have not detected them. The primary debris discovered through using SEM-EDS were calcium and aluminum precipitation, as shown in **Figure 15**. A sample precipitate with EDX spectra of the precipitate and background film is shown in **Figure 16**. Both images were taken from the same perspective, with the darker features being primarily Ca, and the lighter being primarily Ti. This compares to **Figure 12A**, an unexposed film with a lack of surface debris. However, calcium carbonate deposition on the surface does not explain the brown color that developed on the film. Further studies are needed to determine if Ca is the primary foulant in this matrix or if its precipitation is promoted by the same factors (e.g., pH) that promote precipitation of the active catalyst foulants (e.g., Fe, Mn oxide phases).

3.9. Catalyst reactivation and properties post-treatment in GW

From the above results and prior studies, precipitation of cations, in particular, Mn, Fe and Ca, were suspected to be responsible for deactivation of the catalyst. Appropriate regenerating agents were used to attempt reactivation of the catalyst from this knowledge. Ascorbic acid and oxalic acid were selected for their reducing (both agents) and chelating (oxalic) properties. A hydrochloric acid solution of similar pH was also used to determine if acidification was a possible regeneration mechanism. Photocatalysts fouled in the experiment described in **Figure 14** were rinsed in a 1 mM solution of ascorbic or oxalic acid, or a pH 3.5

solution of HCl (matching the pH of the oxalic acid solution). They were then tested in small (2 films) batch reactor systems circulating with the DI water matrix. **Figure 17** describes the results from these experiments. The results indicate that both ascorbic acid and oxalic acid were potential regeneration agents of these fouled catalysts. The HCl solution had some effect, but was not as effective as the ascorbic acid or oxalic acid. This suggests that reduction (by ascorbic acid and oxalic acid) and chelation (by oxalic acid) are important regeneration mechanisms.

Following on the results of the batch systems, a longer experiment was run such that the GW experiment as in **Figure 14** was repeated, followed by a rinse of the reactor with an inlet of 1 mM oxalic acid for 24 h, followed by a return to the DI solution. The results are presented in **Figure 18**. The first 8 d of the experiment was a replicate of the previous experiment, and the trends for each compound were comparable. After oxalic acid wash for 24 h, the brown film was removed from the first four channels of catalysts, with some remaining on the fifth channel. Removal of the brown film was also observed when rinsing in batches. The catalyst was regenerated to nearly the same activity level as was observed in the first 2 d of DI solution.

The catalysts were analyzed post-experiment by SEM-EDS. The oxalic acid rinsed image in **Figure 19**, compared with **Figure 15**, shows a clear decrease in the amount of calcium precipitation. This is in addition to the removal of the brown film, as previously mentioned, which may be attributable to iron and/or manganese. This suggests that oxalic acid may be effective against several potential foulants, but future studies are necessary to determine the exact mechanism of foulant removal from the catalyst. Oxalic acid may be an effective general cleaning agent of TiO_2.

3.10. Effectiveness of pretreatment of GW

Calcium was identified as a potential foulant of the catalysts, as described in the experiments above. Softening of the groundwater was chosen as a potential solution to this problem. GW was softened by raising the pH to 11 with NaOH, filtration to 1 µm, then decreasing the pH to its original value with HCl (in this case, pH 8.35). The calcium concentration decreased from 39 mg/L to 25.4 mg/L. Alkalinity was reduced by roughly 20%. Modeling the process with MINEQL+ indicated a larger amount of Ca could be removed, assuming all precipitated solids were filtered. This indicates that in future studies two options should be explored; a) stir solution at pH 11 for a longer period of time, and/or b) use a smaller

filter (<1 μm). The results of this experiment are described in **Figure 20**. Generally, the catalyst activity is not deactivated as much as in the aerated raw GW. This suggests even a relatively small (35%) reduction in the calcium concentration could decrease or delay inhibition and deactivation, though further studies are needed to make this conclusion.

CONCLUSIONS

In this contribution, we demonstrated a new laboratory benchtop continuous-flow TiO_2 photocatalytic reactor that will be useful for studying critical factors and mechanisms affecting the activity, inhibition, and deactivation of immobilized photocatalysts by non-target water constituents present in diverse matrices that are relevant to the water treatment industry. Through a combination of tracer studies, circulating batch, and continuous-flow experiments, the reactor and photocatalysis behavior were stable and could be modeled as a plug flow reactor model. Photocatalytic degradation rates of micropollutants were inhibited in WWE due to the presence of both organic and inorganic non-target constituents. However, photocatalysts were not deactivated to a large degree after 4 d of continuous treatment of micropollutants in a WWE matrix. This suggests that the technology has promise for advanced treatment applications (e.g., polishing step in potable water reuse systems). Still, longer term studies (e.g., weeks, months) are needed to gain a better understanding of the factors controlling catalyst activity and longevity. In addition, studies are needed to identify the specific photocatalyst-inhibiting agents present in the WWE and assess the feasibility of pretreatment and regenerative strategies for increasing removal of the target micropollutants and extending photocatalyst longevity. Photocatalytic degradation rates of micropollutants displayed different trends on a GW-exposed photocatalyst. Easily oxidizable compounds (APAP and SMX) were little affected by catalyst exposure to GW, while less oxidizable compounds (IOP and CBZ) were significantly inhibited. Further studies are necessary to determine the mechanism(s) responsible for this, and if different pathways are affected by catalyst fouling differently. Oxalic acid was found to be an effective cleaning agent of TiO_2 after exposure to GW. Softening of the GW is a potentially effective pretreatment strategy. Future studies will determine effective pre-treatment strategies for GW, specifically to remove the dominant divalent and trivalent cations (calcium, iron, manganese).

REFERENCES

(1) Oulton, R. L.; Kohn, T.; Cwiertny, D. M. Pharmaceuticals and personal care products in effluent matrices: A survey of transformation and removal during wastewater treatment and implications for wastewater management RID H-1430-2011. *J. Environ. Monit.* **2010**, *12*, 1956–1978.

(2) Ternes, T. A. Occurrence of drugs in German sewage treatment plants and rivers. *Water Research* **1998**, *32*, 3245–3260.

(3) Daughton, C. G.; Ternes, T. A. Pharmaceuticals and personal care products in the environment: Agents of subtle change? *Env. Health. Persp.* **1999**, *107*, 907–938.

(4) Sedlak, D. L.; Gray, J. L.; Pinkston, K. E. Understanding Microcontaminants in Recycled Water. *Environ. Sci. Technol.* **2000**, *34*, 508A–515A.

(5) Zwiener, C.; Frimmel, F. H. Oxidative treatment of pharmaceuticals in water. *Water Research* **2000**, *34*, 1881–1885.

(6) Huber, M. M.; Canonica, S.; Park, G.-Y.; von Gunten, U. Oxidation of Pharmaceuticals during Ozonation and Advanced Oxidation Processes. *Environ. Sci. Technol.* **2003**, *37*, 1016–1024.

(7) Haag, W. R.; Yao, C. C. D. Rate constants for reaction of hydroxyl radicals with several drinking water contaminants. *Environ. Sci. Technol.* **1992**, *26*, 1005–1013.

(8) Ning, B.; Graham, N. J. D. Ozone Degradation of Iodinated Pharmaceutical Compounds. *Journal of Environmental Engineering* **2008**, *134*, 944–953.

(9) Anquandah, G.; Ray, M. B.; Ray, A. K.; Al-Abduly, A. J.; Sharma, V. K. Oxidation of X-ray compound ditrizoic acid by ferrate(VI). *Environmental Technology* **2011**, *32*, 261–267.

(10) Kalsch, W. Biodegradation of the iodinated X-ray contrast media diatrizoate and iopromide. *Science of The Total Environment* **1999**, *225*, 143–153.

(11) Calza, P.; Medana, C.; Pazzi, M.; Baiocchi, C.; Pelizzetti, E. Photocatalytic transformations of sulphonamides on titanium dioxide. *Appl. Catal. B* **2004**, *53*, 63–69.

(12) Doll, T. E.; Frimmel, F. H. Photocatalytic degradation of carbamazepine, clofibric acid and iomeprol with P25 and Hombikat UV100 in the presence of natural organic matter (NOM) and other organic water constituents. *Water Res.* **2005**, *9*, 403–411.

(13) Ohko, Y.; Iuchi, K.-I.; Niwa, C.; Tatsuma, T.; Nakashima, T.; Iguchi, T.; Kubota, Y.; Fujishima, A. 17α-Estradiol degradation by TiO2 photocatalysis as a means of reducing estrogenic activity. *Environ. Sci. Technol.* **2002**, *36*, 4175–4181.

(14) Valencia, S.; Marín, J. M.; Restrepo, G. Study of the bandgap of synthesized titanium dioxide nanoparticules using the sol-gel method and a hydrothermal treatment. *Open Materials Science Journal* **2010**, *4*, 9–14.

(15) Doll, T. E.; Frimmel, F. H. Removal of selected persistent organic pollutants by heterogeneous photocatalysis in water. *Catalysis Today* **2005**, *101*, 195–202.

(16) Hoffmann, M. R.; Martin, S. T.; Choi, W.; Bahnemann, D. W. Environmental Applications of Semiconductor Photocatalysis. *Chem. Rev.* **1995**, *95*, 69–96.

(17) Zhang, Y.; Crittenden, J. C.; Hand, D. W.; Perram, D. L. Fixed-bed photocatalysts for solar decontamination of water. *Environ. Sci. Technol.* **1994**, *28*, 435–442.

(18) Mitoraj, D.; Kisch, H. The Nature of Nitrogen-Modified Titanium Dioxide Photocatalysts Active in Visible Light. *Angewandte Chemie International Edition* **2008**, *47*, 9975–9978.

(19) Klamerth, N.; Miranda, N.; Malato, S.; Agüera, A.; Fernández-Alba, A. R.; Maldonado, M. I.; Coronado, J. M. Degradation of emerging contaminants at low concentrations in MWTPs effluents with mild solar photo-Fenton and TiO2. *Catalysis Today* **2009**, *144*, 124–130.
(20) Rizzo, L.; Meric, S.; Guida, M.; Kassinos, D.; Belgiorno, V. Heterogenous photocatalytic degradation kinetics and detoxification of an urban wastewater treatment plant effluent contaminated with pharmaceuticals. *Water Research* **2009**, *43*, 4070–4078.
(21) Doll, T. E.; Frimmel, F. H. Kinetic study of photocatalytic degradation of carbamazepine, clofibric acid, iomeprol and iopromide assisted by different TiO2 materials—determination of intermediates and reaction pathways. *Water Research* **2004**, *38*, 955–964.
(22) Choina, J.; Duwensee, H.; Flechsig, G.-U.; Kosslich, H.; Morawski, A. W.; Tuan, V. A.; Schulz, A. Removal of hazardous pharmaceutical from water by photocatalytic treatment. *Central European Journal of Chemistry* **2010**, *8*, 1288–1297.
(23) Miranda-García, N.; Suárez, S.; Sánchez, B.; Coronado, J. M.; Malato, S.; Maldonado, M. I. Photocatalytic degradation of emerging contaminants in municipal wastewater treatment plant effluents using immobilized TiO2 in a solar pilot plant. *Applied Catalysis B: Environmental* **2011**, *103*, 294–301.
(24) Nano, G. V.; Strathmann, T. J. Application of Surface Complexation Modeling to the Reactivity of Iron(II) with Nitroaromatic and Oxime Carbamate Contaminants. *J. Colloid Interface Sci.* **2008**, *321*, 350–359.
(25) Balasubramanian, G.; Dionysiou, D.; Suidan, M.; Subramanian, Y.; Baudin, I.; Laine, J. Titania powder modified sol-gel process for photocatalytic applications. *J. Mater. Sci.* **2003**, *38*, 823–831.
(26) Hatchard, C. G.; Parker, C. A. A New Sensitive Chemical Actinometer: Potassium Ferrioxalate as a Standard Chemical Actinometer. *Proc. R. Soc. Lond. A* **1956**, *235*, 518–536.
(27) Eaton, A. D.; Franson, M. A. H.; Association, A. W. W.; Federation, W. E. *Standard methods for the examination of water & wastewater*; American Public Health Association, 2005.
(28) Balasubramanian, G.; Dionysiou, D. D.; Suidan, M. T.; Baudin, I.; Laîné, J.-M. Evaluating the activities of immobilized TiO2 powder films for the photocatalytic degradation of organic contaminants in water. *Applied Catalysis B: Environmental* **2004**, *47*, 73–84.
(29) Chen, Y.; Dionysiou, D. D. TiO2 photocatalytic films on stainless steel: The role of Degussa P-25 in modified sol–gel methods. *Applied Catalysis B: Environmental* **2006**, *62*, 255–264.
(30) Clark, M. M. *Transport modeling for environmental engineers and scientists*; Wiley-Interscience, 2009.
(31) Canonica, S.; Kohn, T.; Mac, M.; Real, F. J.; Wirz, J.; Von Gunten, U. Photosensitizer Method to Determine Rate Constants for the Reaction of Carbonate Radicals with Organic Compounds. *Environ. Sci. Technol.* **2005**, *39*, 9182–9188.
(32) Paul, T.; Miller, P. L.; Strathmann, T. J. Visible-Light-Mediated TiO2 Photocatalysis of Fluoroquinolone Antibacterial Agents. *Environ. Sci. Technol.* **2007**, *41*, 4720–4727.

(33) Burns, R. A.; Crittenden, J. C.; Hand, D. W.; Selzer, V. H.; Sutter, L. L.; Salman, S. R. Effect of Inorganic Ions in Heterogeneous Photocatalysis of TCE. *Journal of Environmental Engineering* **1999**, *125*, 77–85.

FIGURES AND TABLES

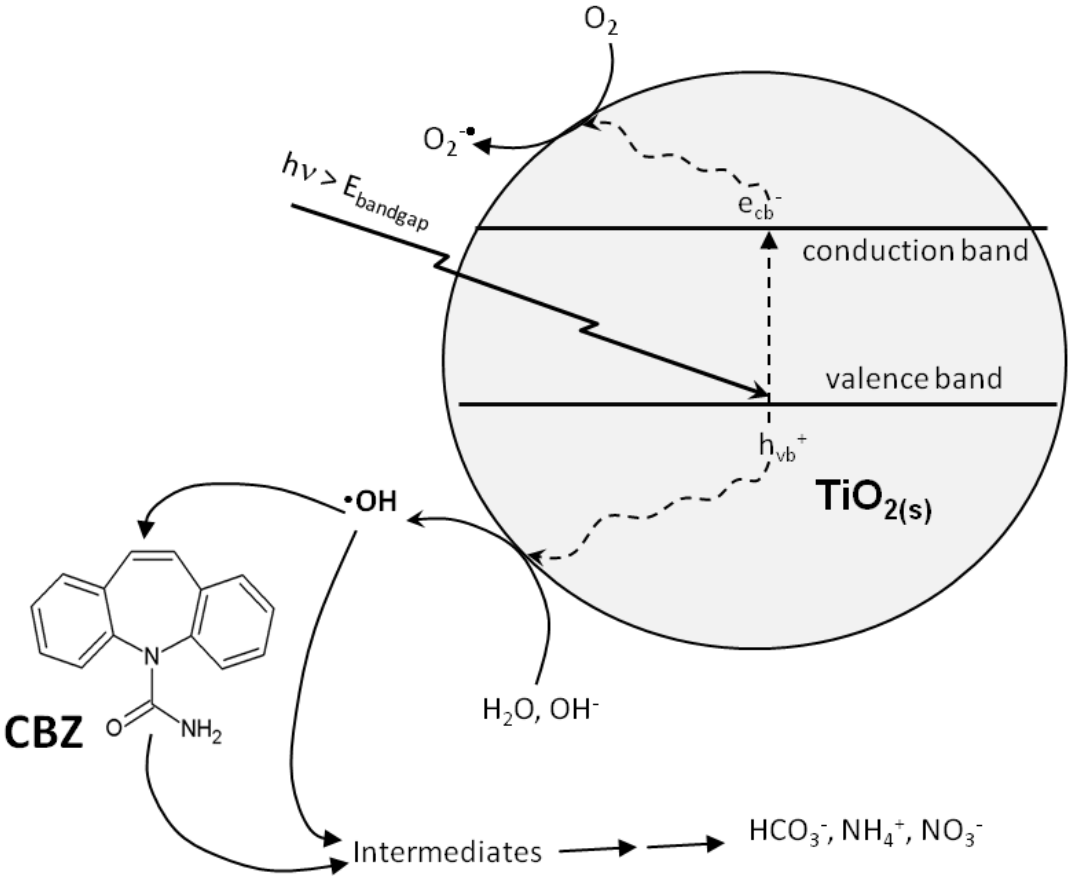

Figure 1. Simplified representation of UV-TiO_2 photo-excitation mechanism and its application for oxidation of pharmaceutical micropollutants like carbamazepine (CBZ).

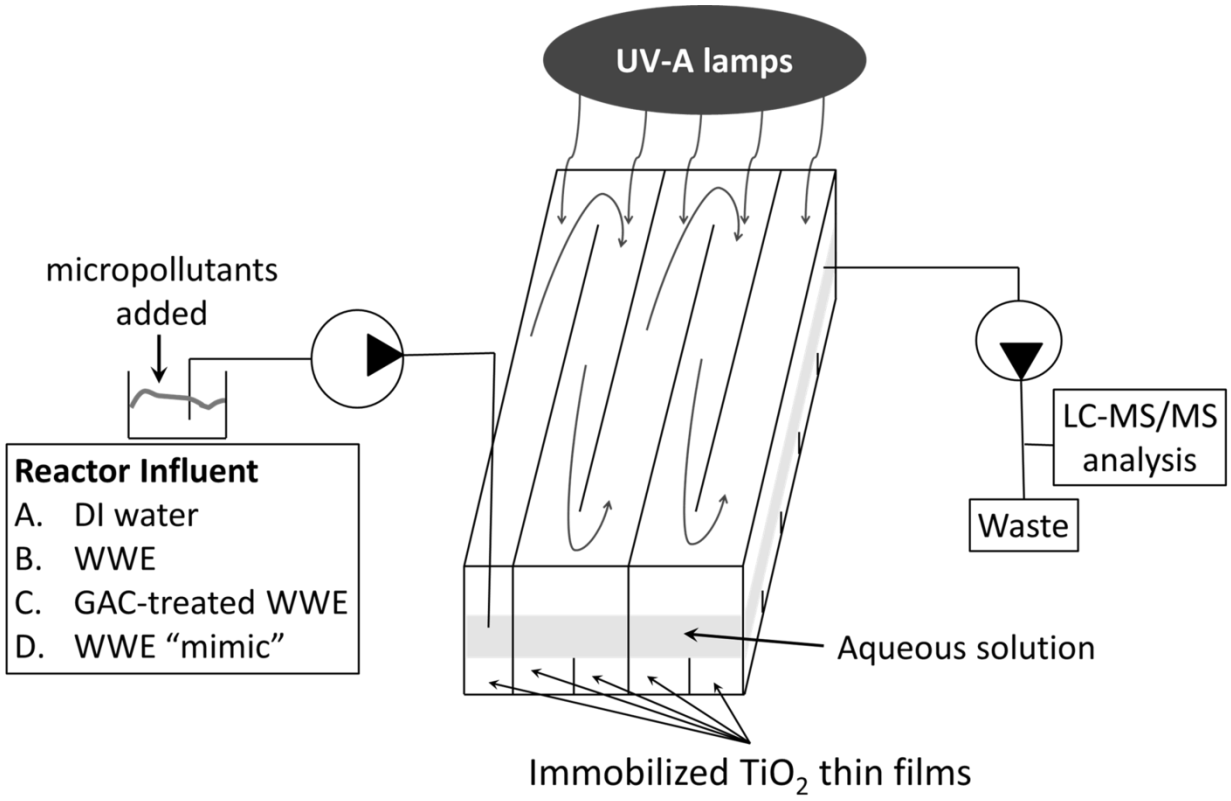

Figure 2. Schematic of continuous-flow reactor and list of influent feed solutions examined in study.

Compound	Structure	Common usage(s)
Acetaminophen (APAP)	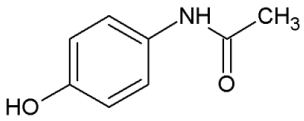	analgesic
Carbamazepine (CBZ)	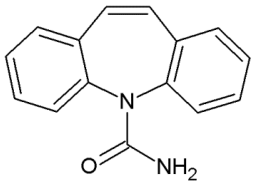	analgesic, antiepileptic
Iopromide (IOP)	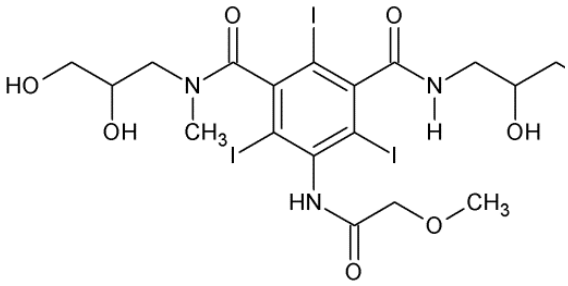	X-ray contrast agent
Sulfamethoxazole (SMX)	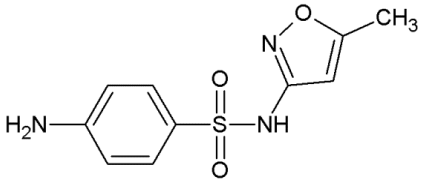	antibiotic

Figure 3. Micropollutants used in study.

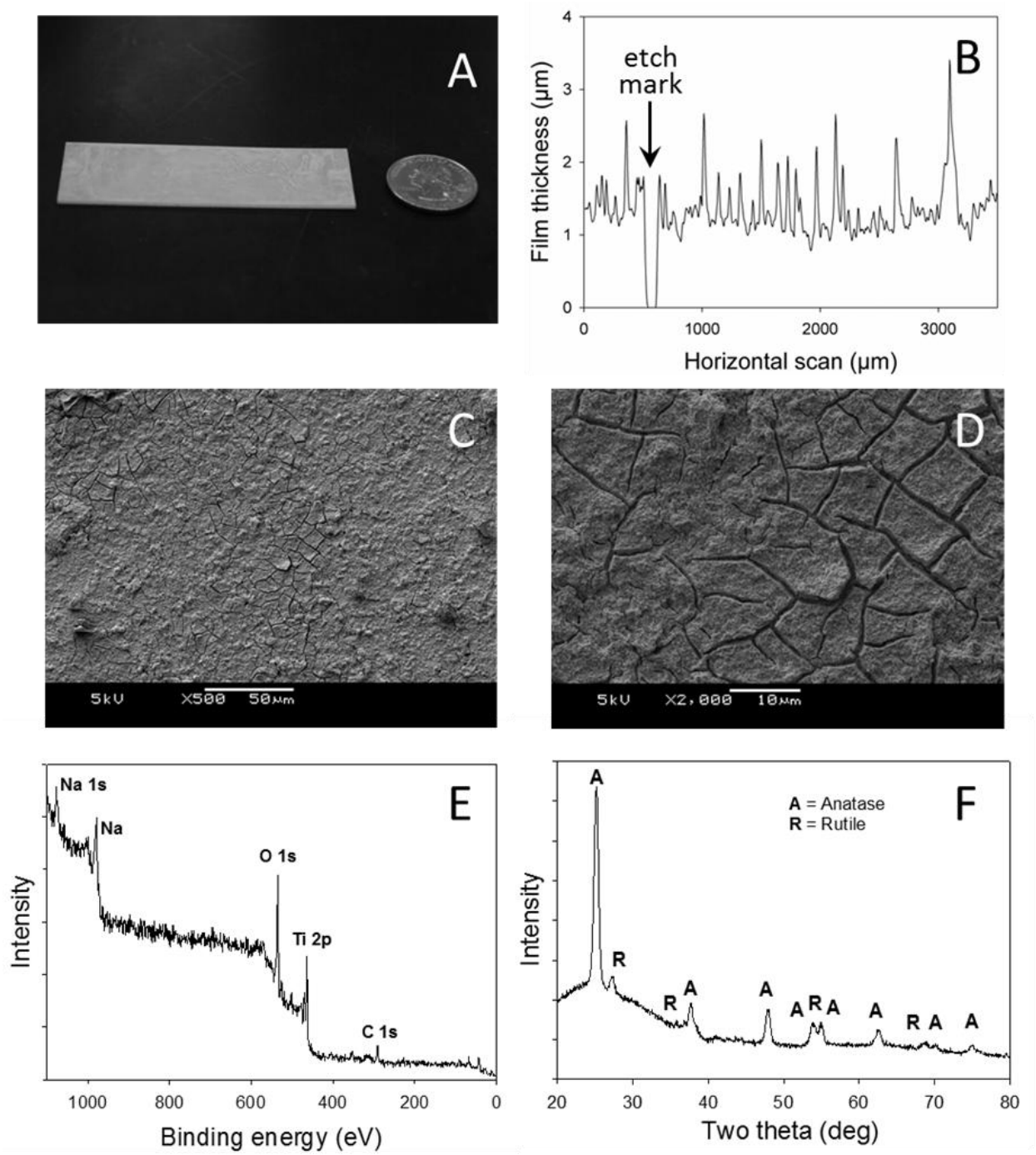

Figure 4. Characterization of virgin TiO_2 photocatalyst including photograph with comparison to US quarter (A), profilometry (B), representative SEM micrographs at two different magnifications (C-D), x-ray diffractogram (E), and X-ray photoelectron spectra (F). Profilometry shows etch in film at x = ~600 μm.

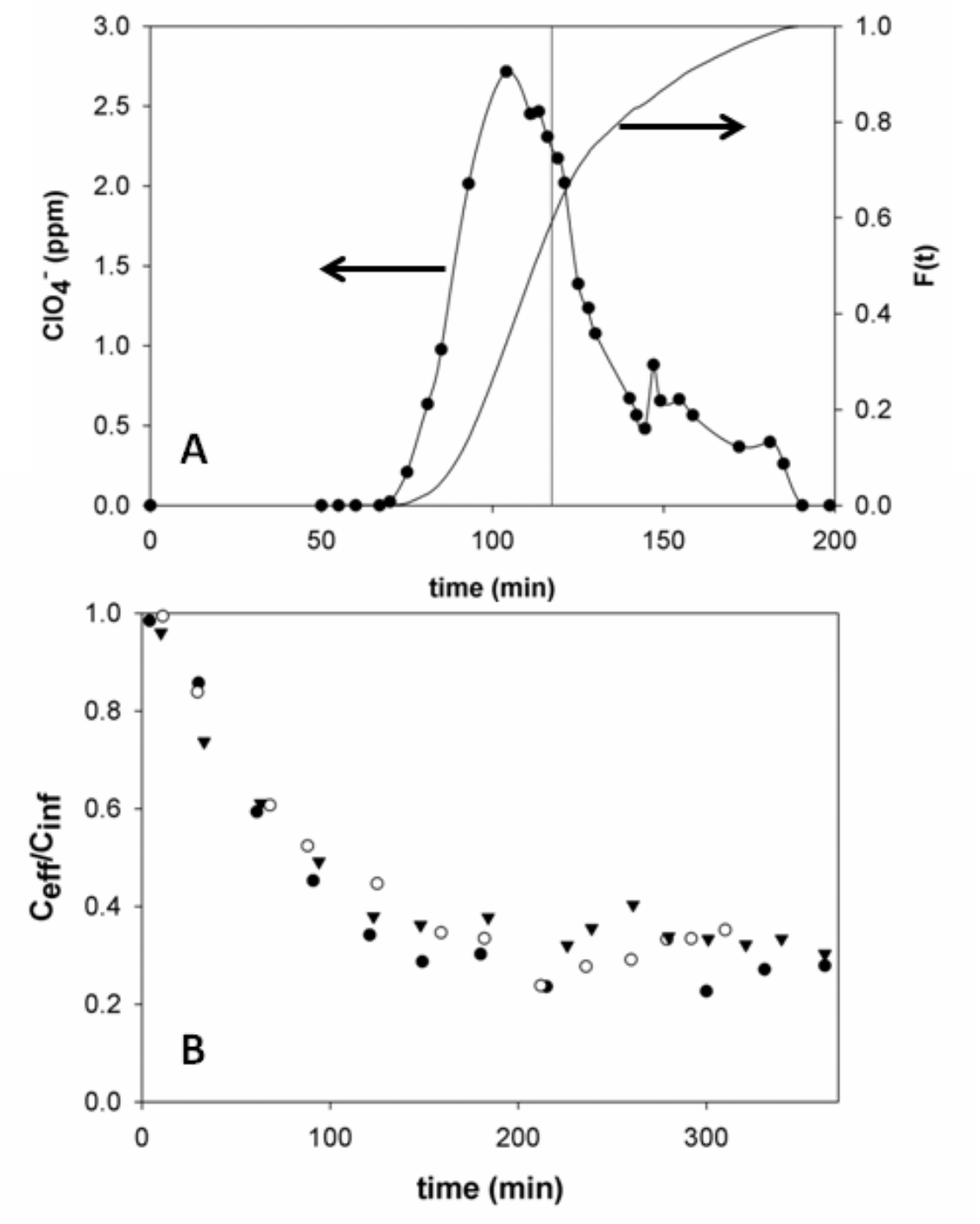

Figure 5. (A) Reactor outlet concentration of ClO_4^- tracer and cumulative tracer function F(t); vertical line indicates measured mean residence time (τ = 117 min). (B) Initial continuous-flow reactor data for photocatalytic treatment of IOP establishing a steady-state level of treatment; different symbols represent individual replicate experiments.

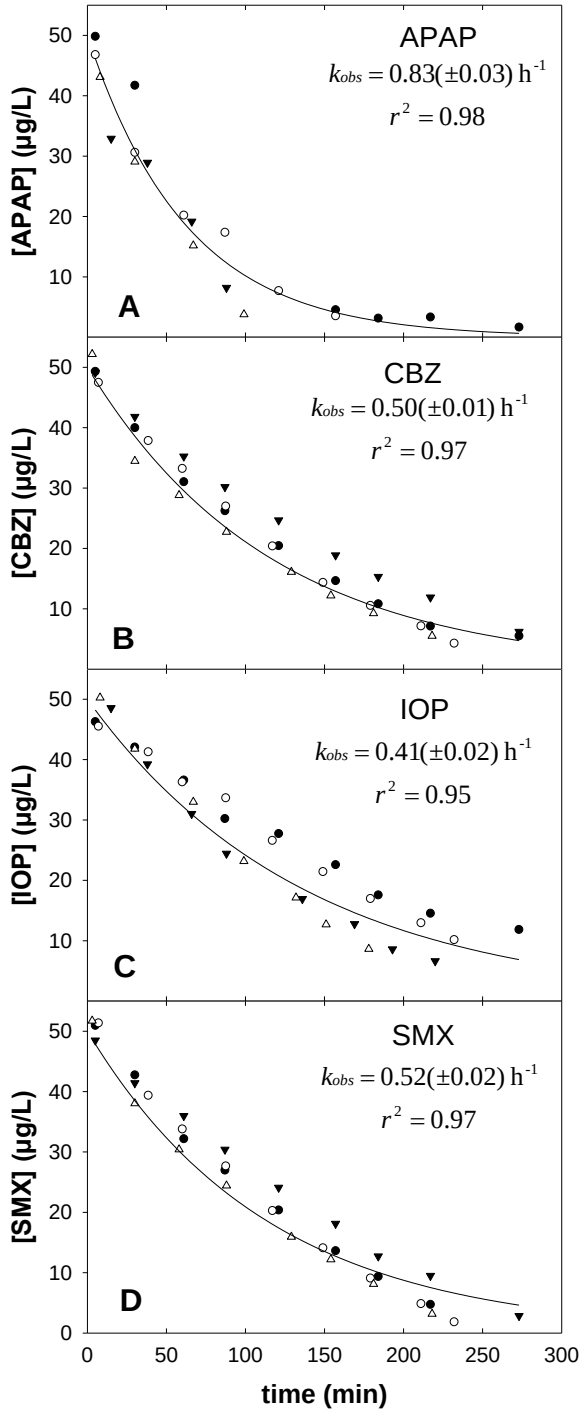

Fig. 6. Circulating batch photocatalytic degradation kinetics of the four micropollutants in the buffered DI water matrix. Individual experiments are represented by different symbols. Fit-derived k_{obs} values and associated uncertainties (1σ) derived from regression of the combined data set for each compound.

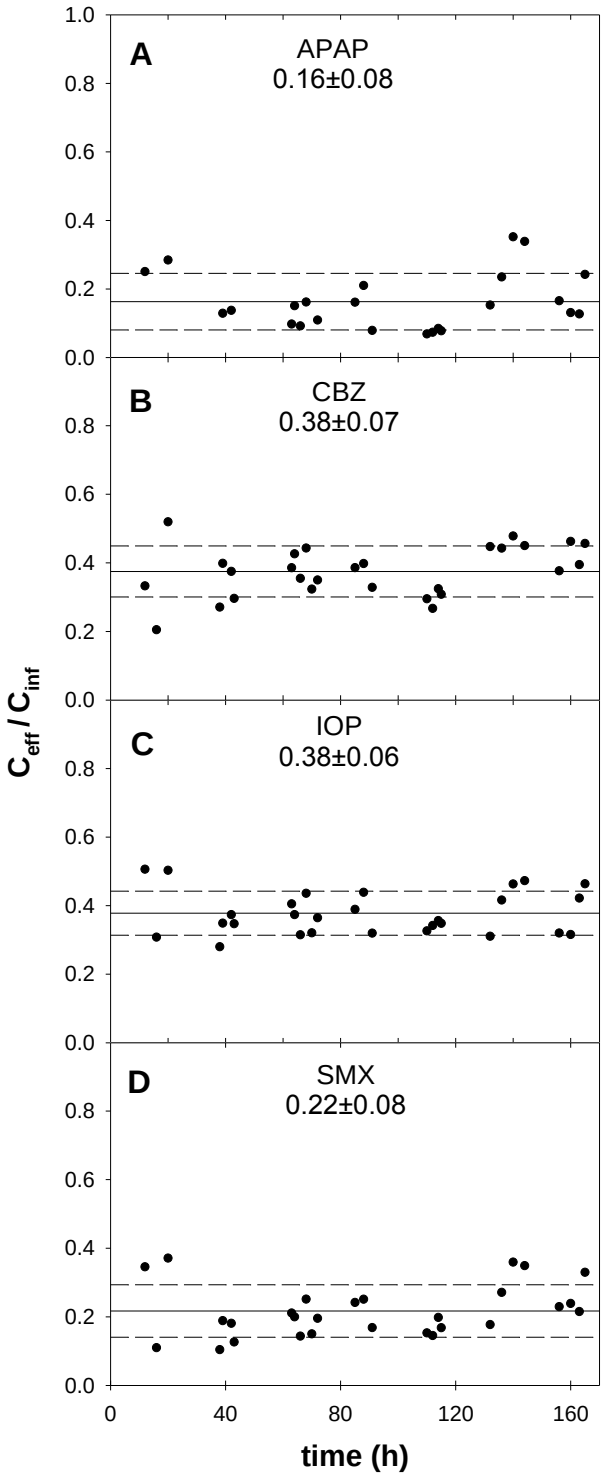

Figure 7. Treatment level for each micropollutant over a 7 day period. Mean and standard deviation indicated with solid and dotted lines, respectively.

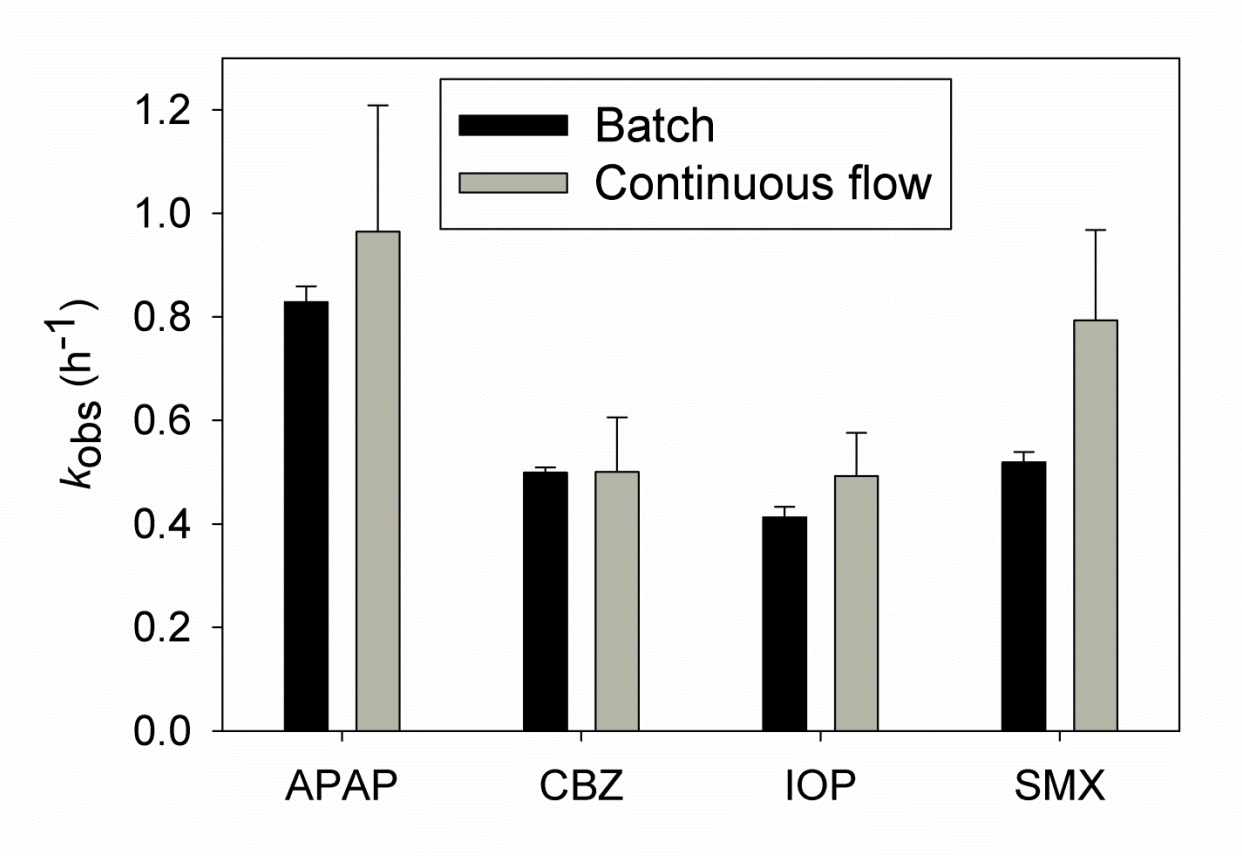

Figure 8. Comparison of k_{obs} values for the target micropollutants determined in circulating batch experiments (Figure 6) and 7-day continuous-flow experiments (Figure 7). Uncertainty = 1σ.

Table 1. WWE Characteristics[a]

Parameter	Concentration
pH	8.2
Alkalinity	104 mg/L as $CaCO_3$
TDS	427 mg/L
DOC	5.7 mg C/L
Dissolved Cations	Na (79.8 mg/L), Ca (28.9 mg/L), Mg (21.5 mg/L), K (8.0 mg/L), Si (4.59 mg/L), P (2.84 mg/L), Br (0.18 mg/L), Sr (0.15 mg/L), Fe (0.12 mg/L), Zn (0.06 mg/L), Ba (0.04 mg/L), Al (0.02 mg/L), Mo (0.01 mg/L), Mn (0.01 mg/L), Li (8 µg/L), Cu (6 µg/L), I (6 µg/L), Rb (5 µg/L), Ni (4 µg/L), Cr (3 µg/L), Se (3 µg/L), Cs (3 µg/L), Ti (2 µg/L), V (2 µg/L), As (2 µg/L), B (1 µg/L), Sn (1 µg/L), Pb (1 µg/L), U (1 µg/L)
Dissolved Anions	0.96 mM NO_3^- , 2.3 mM SO_4^{2-}, 1.76 mM Cl^-, 0.057 mM PO_4^{3-}

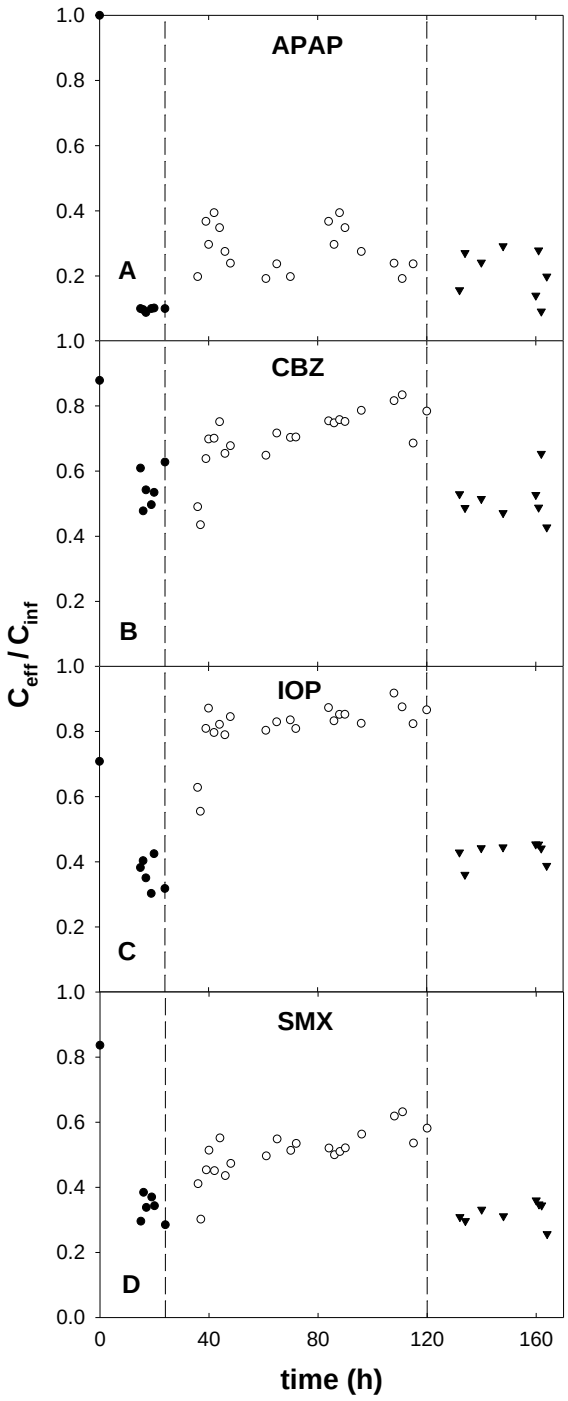

Figure 9. Representative experiment showing removal of the four target micropollutants in the DI water matrix (●), WWE (○), and returning to DI water matrix (▼). Vertical dashed lines indicate time of inlet switching.

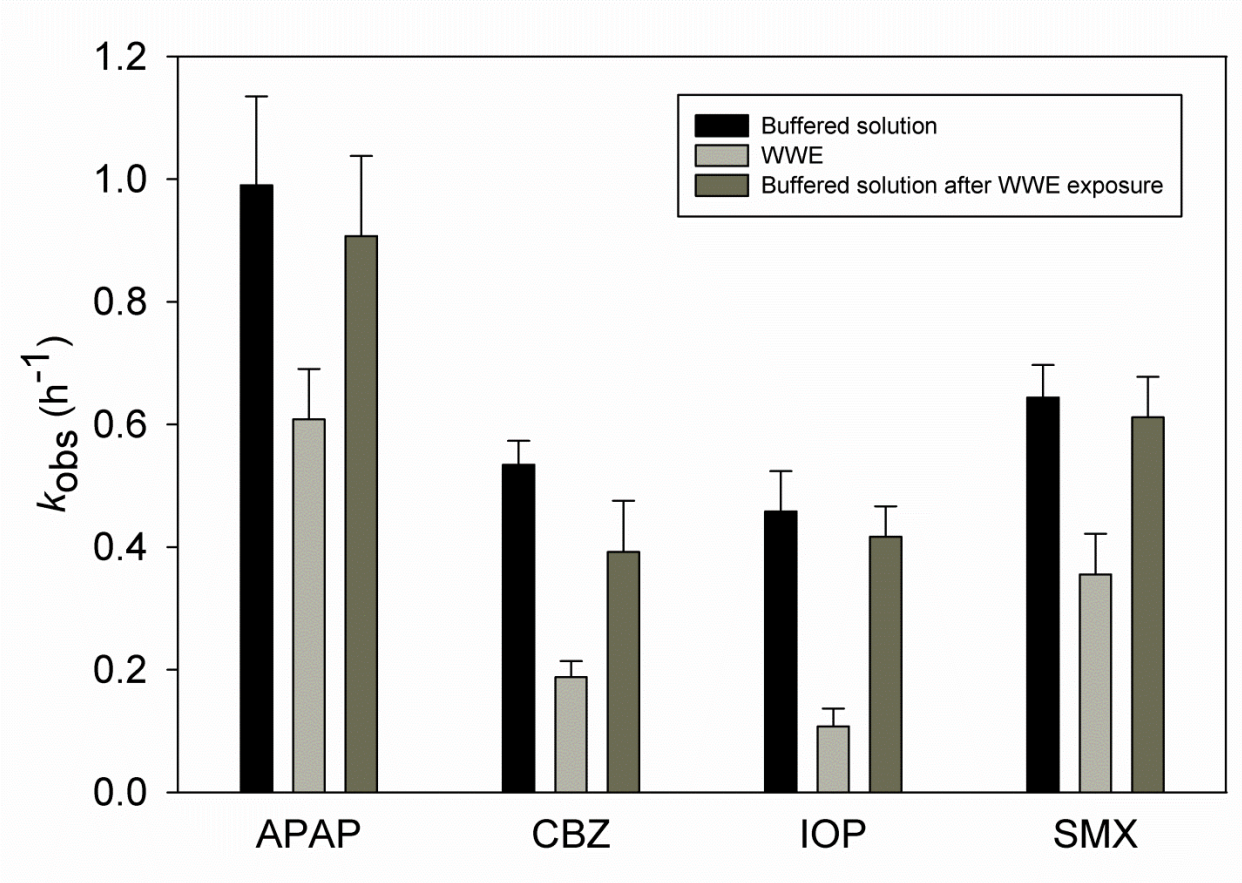

Fig. 10. Mean k_{obs} values for each micropollutant before, during, and after exposure to WWE. Uncertainty = 1σ.

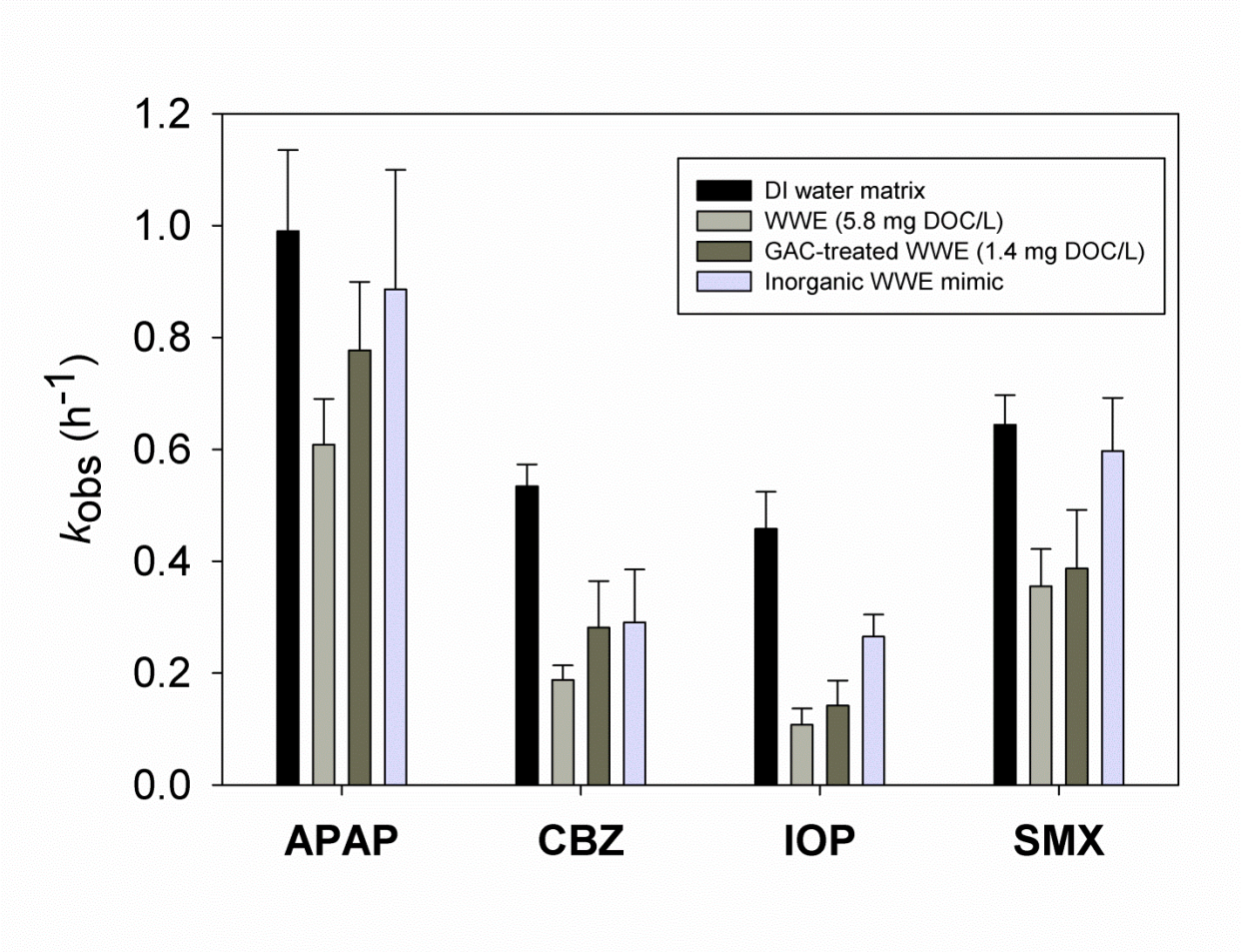

Figure 11. Comparison of observed reaction rate constants in micropollutant-spiked buffered solution, WWE, GAC-treated WWE, and in a laboratory "mimic" solution of inorganic components in WWE. Uncertainty = 1σ.

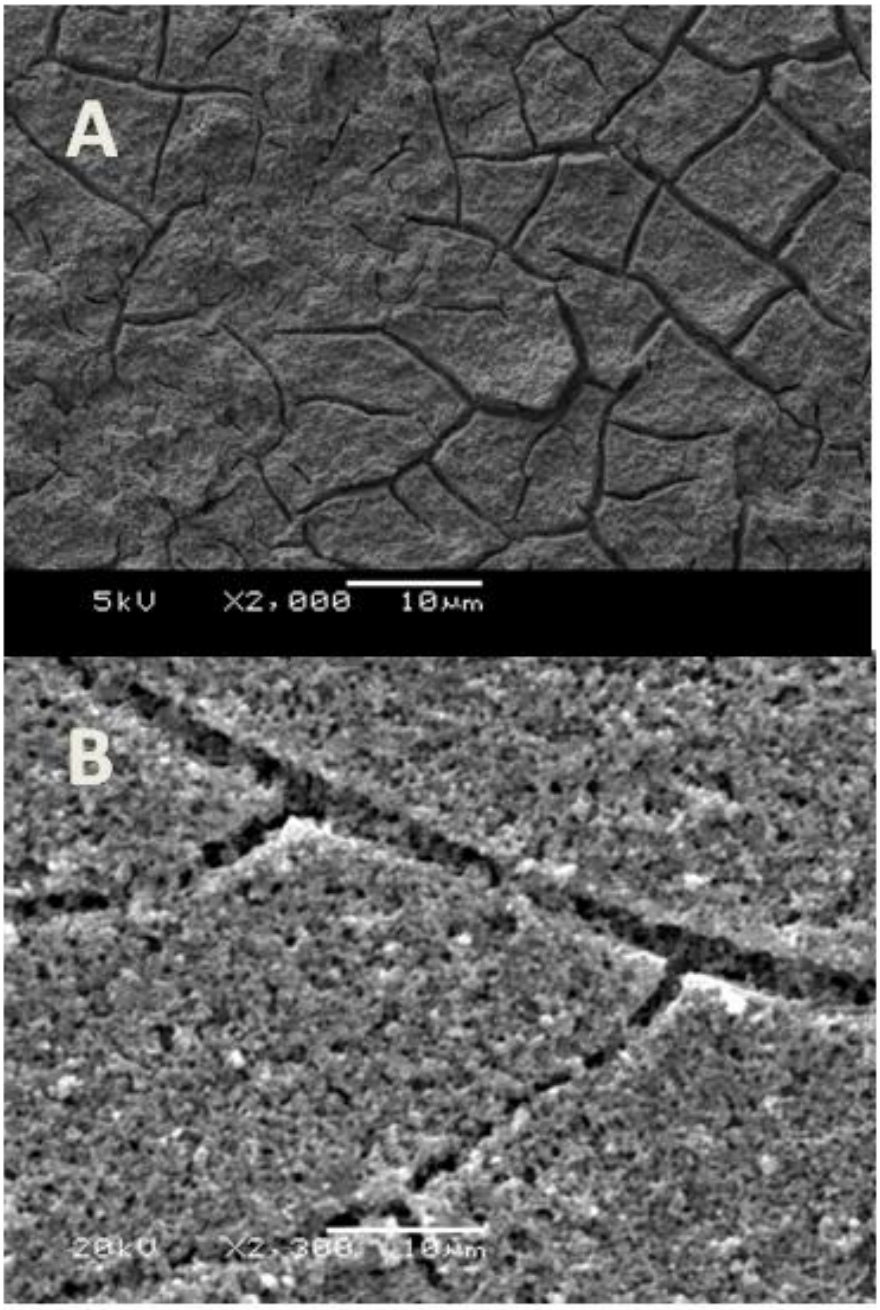

Figure 12. Scanning electron micrograph of (A) unexposed TiO_2 film, (B) TiO_2 film following 4 d of exposure to WWE matrix when treating micropollutants.

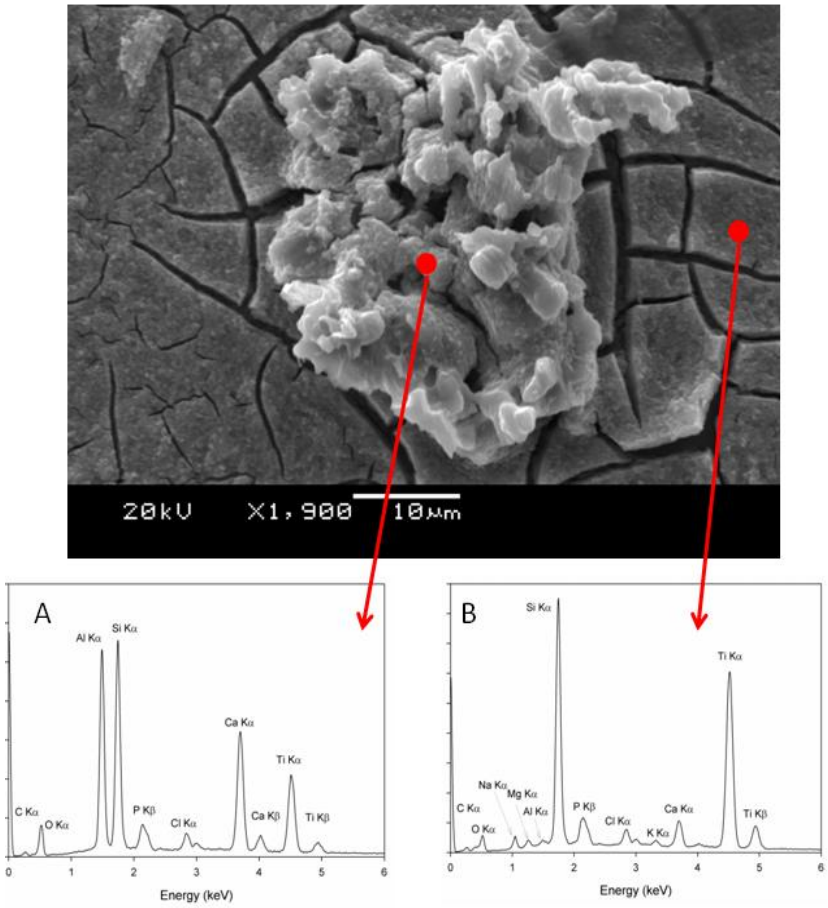

Figure 13. Scanning electron micrograph of precipitate formed during exposure to WWE with EDX spectra of A) precipitate, and B) background film

Table 2. Aerated GW Characteristics[a]

Parameter	Concentration
pH	8.3
Alkalinity	192 mg/L as $CaCO_3$
DOC	2.9 mg C/L
Dissolved Cations	Na (39.8 mg/L), Mg (39.3 mg/L), Ca (39 mg/L), Si (13 mg/L), K (1.95 mg/L), Sr (0.38 mg/L), Ba (0.17 mg/L), Fe (0.061 mg/L), Mn (0.025 mg/L), P (0.012 mg/L), Cu (5 µg/L), Zn (4 µg/L), Cr (3 µg/L), Mo (1 µg/L)

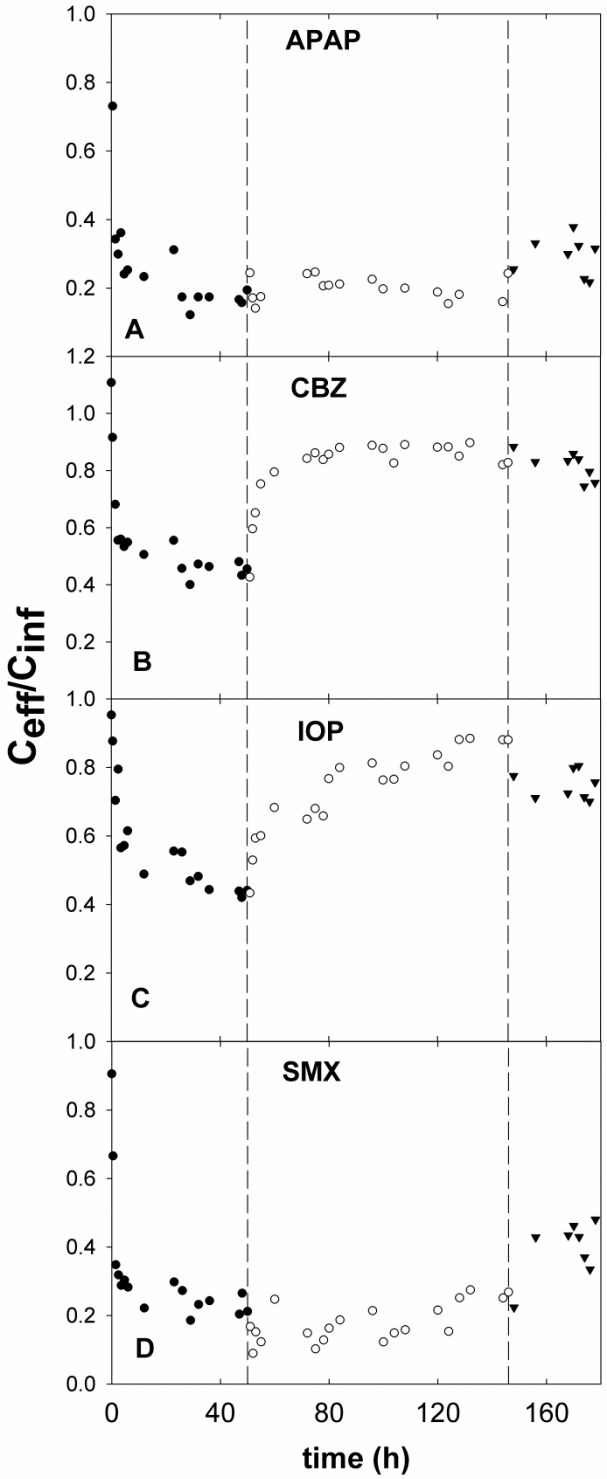

Figure 14. Experiment showing removal of the four target micropollutants in the DI water matrix (●), GW (○), and returning to DI water matrix (▼). Vertical dashed lines indicate time of inlet switching.

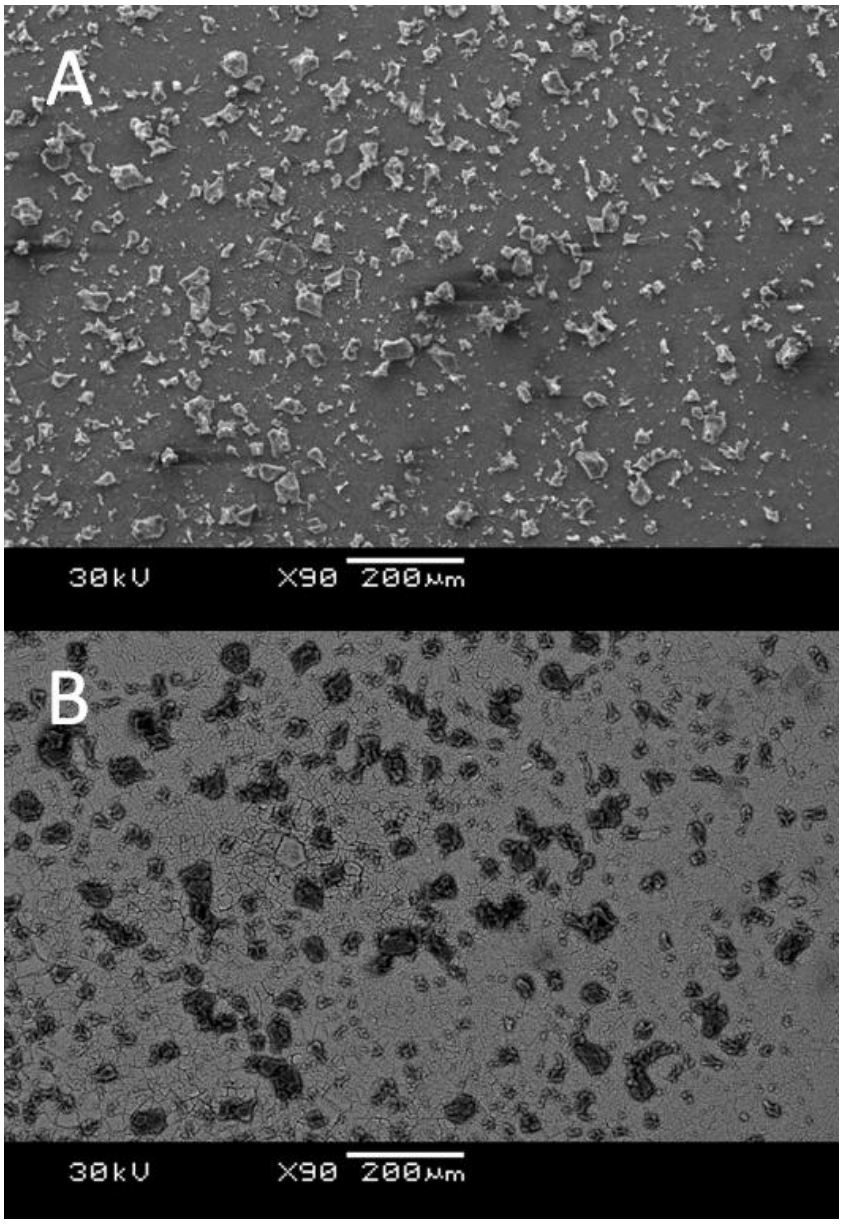

Figure 15. Scanning electron micrograph of (A) TiO_2 film following 4 d of exposure to GW matrix when treating micropollutants, (B) same image in compositional mode. Darker features are lighter elements.

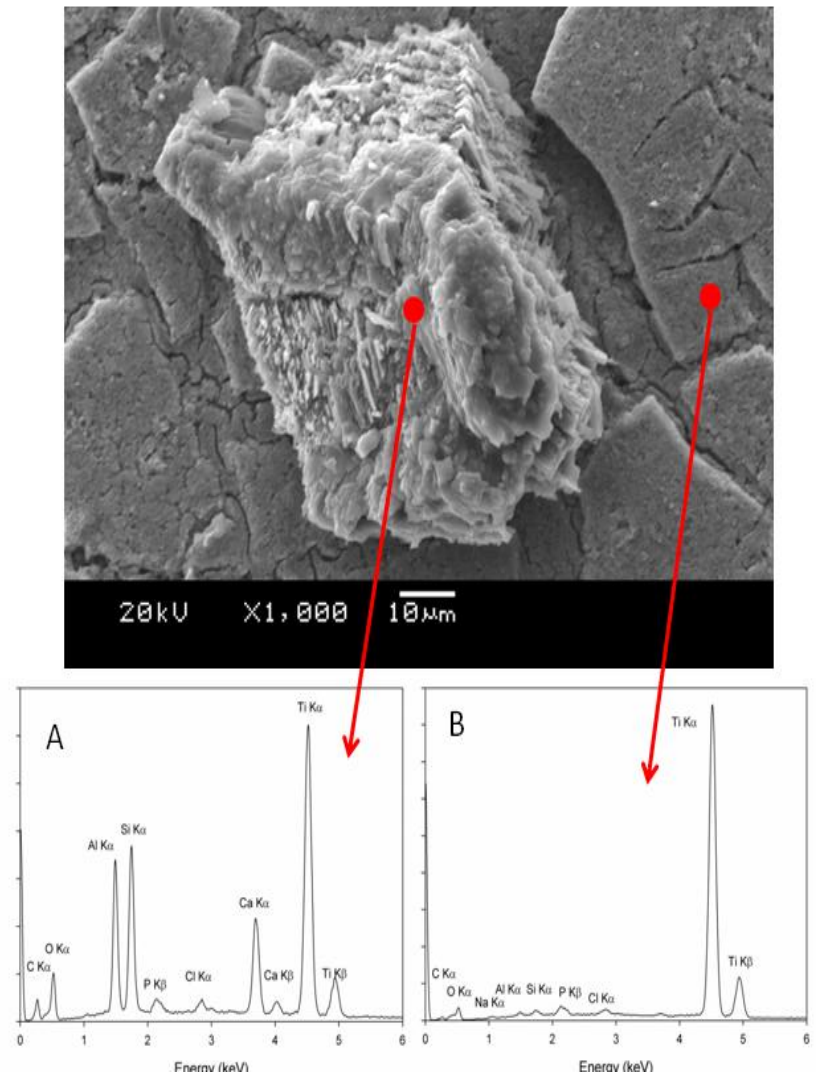

Figure 16. Scanning electron micrograph of precipitate formed during exposure to GW with EDX spectra of A) precipitate, and B) background film

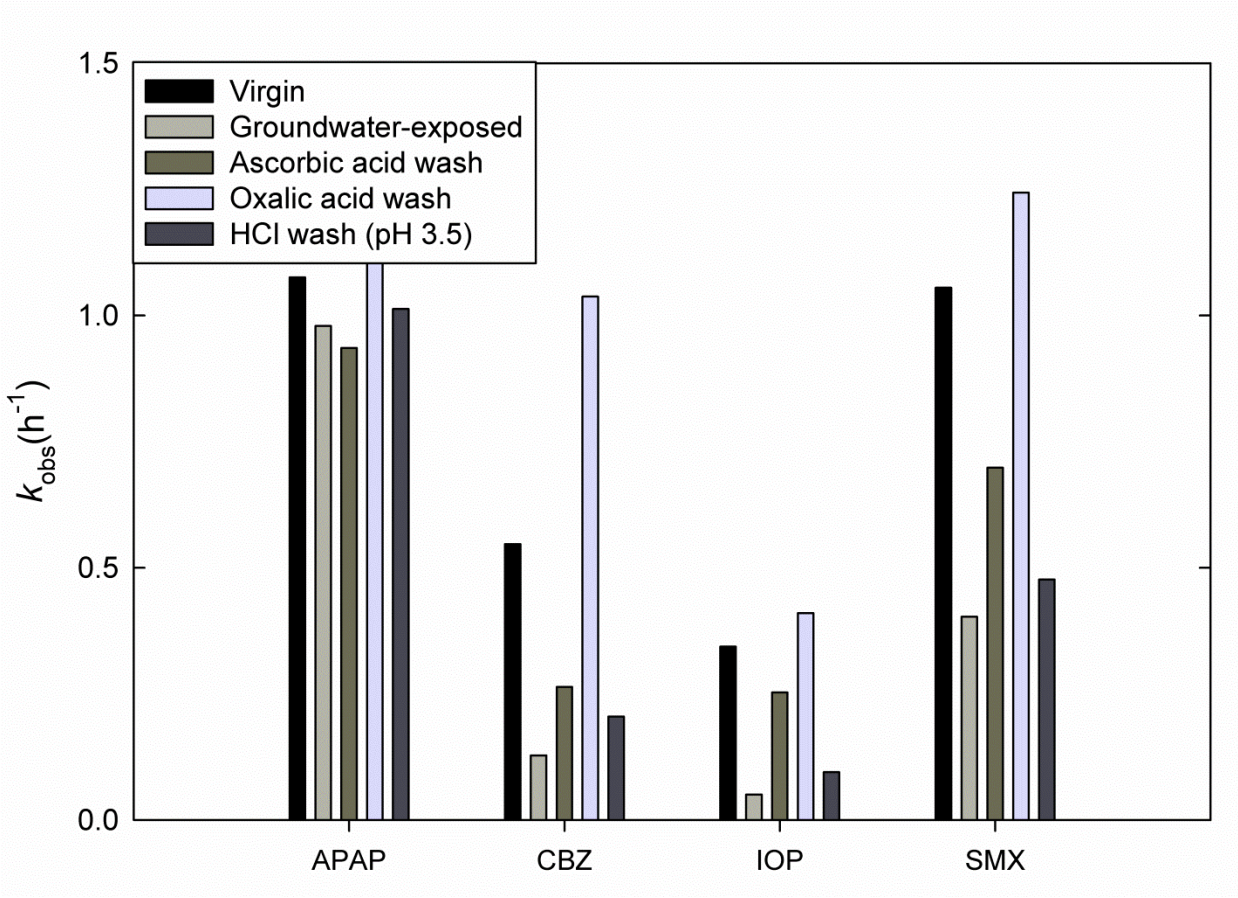

Figure 17. Degradation rates of micropollutants after regeneration of fouled photocatalysts by different rinsing agents. The ascorbic acid and oxalic acid washes were 1 mM.

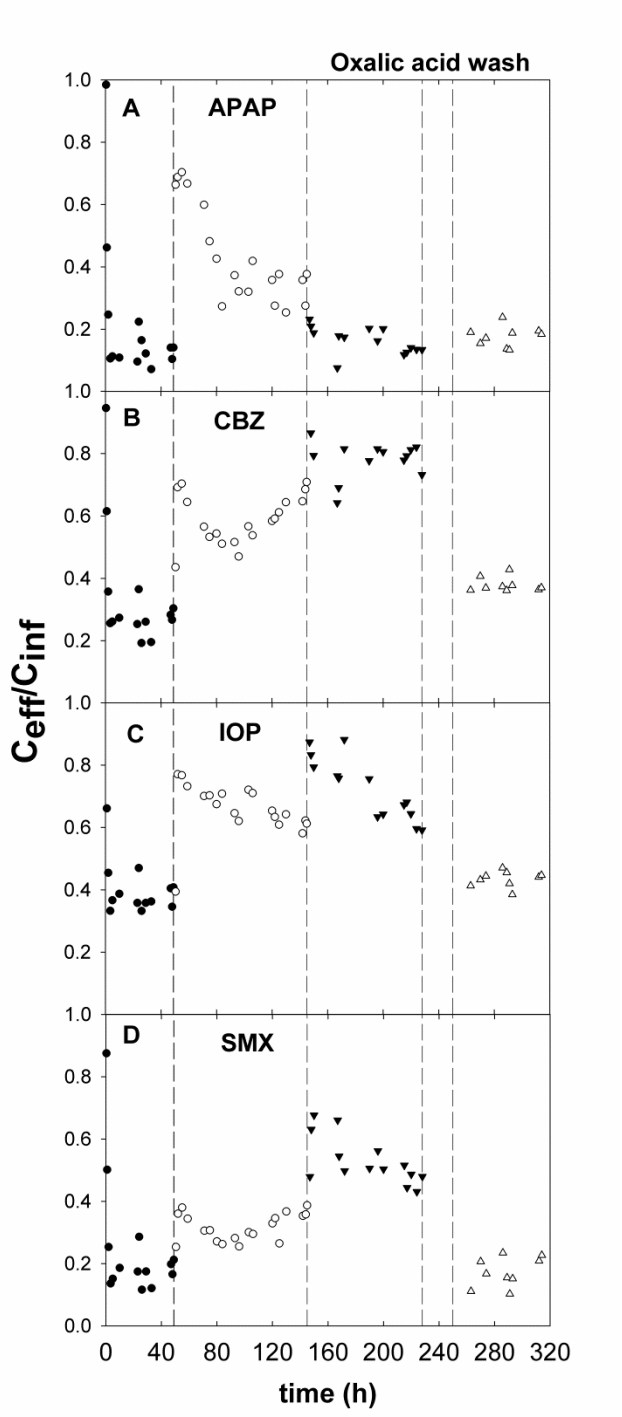

Figure 18. Representative experiment showing removal of the four target micropollutants in the DI water matrix (●), GW (○), returning to DI water matrix (▼), and DI water matrix after oxalic acid rinse (Δ) Vertical dashed lines indicate time of inlet switching. Oxalic acid wash is from period of 228 h to 252 h.

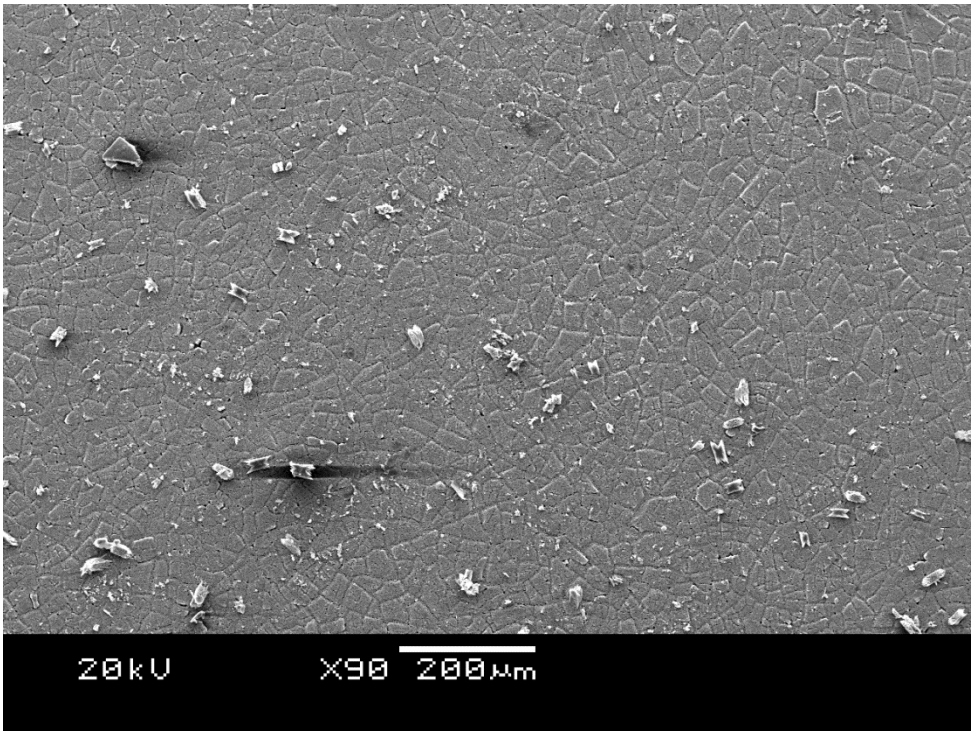

Figure 19. Scanning electron micrograph of TiO_2 film following 4 d of exposure to GW matrix when treating micropollutants, then 1 d of rinsing with oxalic acid.

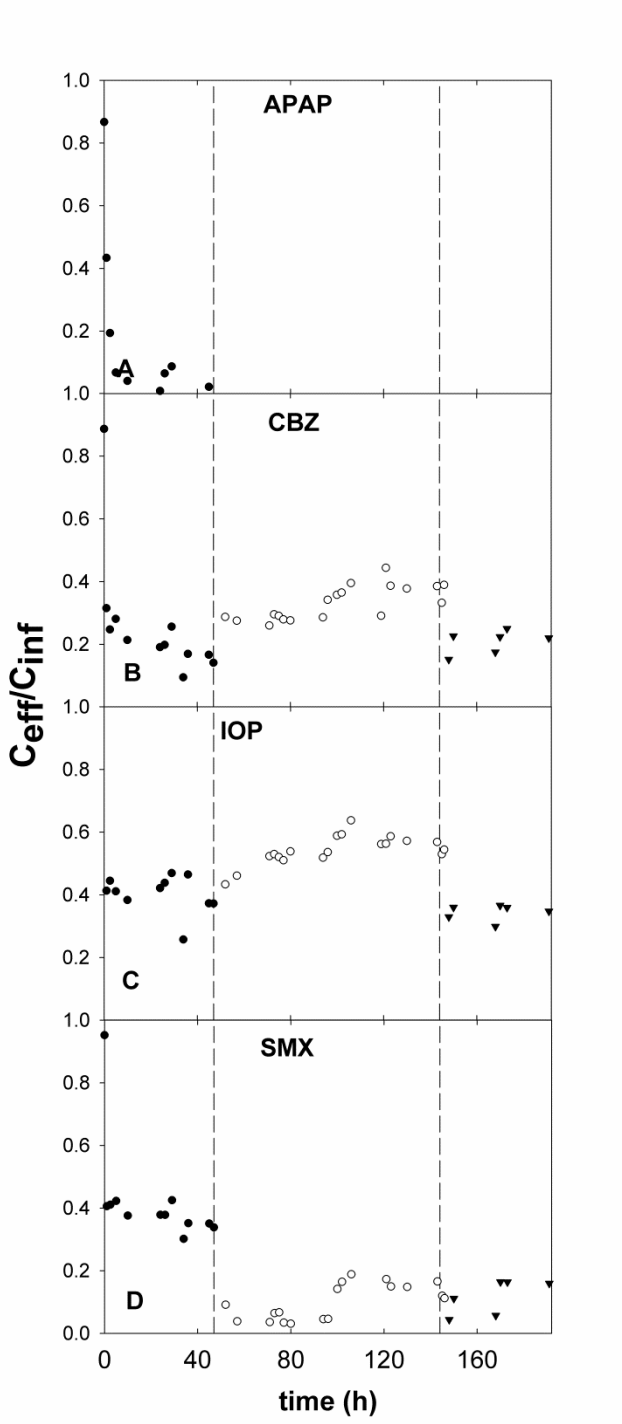

Figure 20. Experiment showing removal of the four target micropollutants in the DI water matrix (●), softened GW (○), and returning to DI water matrix (▼).Vertical dashed lines indicate time of inlet switching. Note: APAP was degraded below detection limit after reaching steady state in DI.

APPENDIX

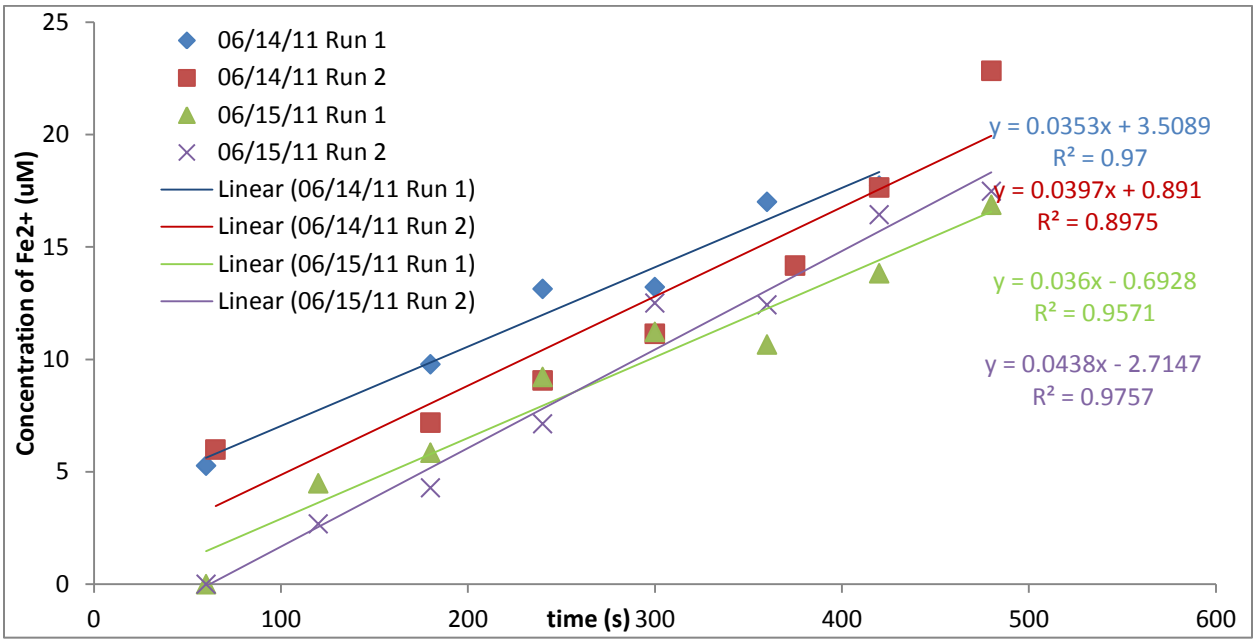

Figure A.1. Compilation of raw data from four actinometry experiments.